Mathematical Modelling of Manufacturing Processes for Control

Jeremy Minton
Supervisor: Dr. Ed Brambley

November 21, 2015

Abstract

Computer numerical control (CNC) has opened numerous opportunities through flexible and low volume manufacturing. 3D-printing and milling are by far the most well known examples as these have been widely adopted in industry. Flexible modification processes - as opposed to additive or subtractive - have not yet seen such success as they are much less predictable; generally large production runs are required to justify the many test runs and specialised tooling required for such processes. To be able to quickly predict the response of a workpiece would make CNC forming a possibility but current design approaches such as numerical simulations are too slow. Modern mathematical techniques could achieve these requirements with approximate solutions.

Assuming a sufficiently thin workpiece, asymptotic analysis has been used to develop four such solutions for two-dimensional sheet rolling. The first is similar to existing solutions in literature but is used to compare these solutions and discuss their limitations. It assumes top to bottom symmetry and a very simple material model, rigid perfectly-plastic. Two different descriptions of friction are applied, Coulomb friction and relative-slip friction. A comparison is also made to numerical solutions, although, numerical simulations were found to perform poorly well with such thin sheets.

Three variations to this first model are also presented. Asymmetry is broken by making the size of the rolls, the rotational speed of the rolls and the strength of friction unequal. This solution was more successfully compared to numerical results and the trends over varying degrees of asymmetry were found to have good agreement.

Next, a more complex material is introduced, which hardens as it is deformed: strain-rate hardening. Finally, the workpiece is assumed to be comprised of two different perfectly-plastic materials bonded together: clad sheet rolling.

The report concludes with some considerations of future work to be conducted.

Preface

The following constitutes the work towards the requirements of a PhD completed to date. The majority of this report, sections 4 and 5, is based on the fourth-term report I submitted in October 2014 as an intermediary progress assessment. Both these sections have been expanded to include greater detail, however, more significant is the addition of sections 6 and 7.

Sections 1 to 3 contain background, review material and the relevant governing equations. The following four sections contain original material. Similarities to existing work is strong in parts, such as section 4. This is discussed at the end of that section where the validity and viability of existing models are examined in relation to new model presented. Sections 5 to 7 present asymmetric models that extend and generalise considerably from the one publication on this topic.

I would like to acknowledge my supervisor Dr. E. J. Brambley for his guidance and support as well as Dr. C. J. Cawthorn for much discussion and advice.

Statement by Jeremy Minton:

Endorsed by Dr. E.J. Brambley:

1 Introduction

For much of human history, manufacturing relied on skilled artisans to hand produce single items. The industrial revolution introduced machine-based manufacturing and then developments in mass production led to item creation being divided into many small processes for automation or greater labourer mastery. Machines are now able to accomplish nearly every step of a manufacturing process.

Manufacturing management strategies, such as *just-in-time* manufacturing and recent market trends for customisability, have increased the demand for flexible, yet still highly automated processes. Computer numerical control (CNC) machines have met that demand and are now common place in additive and subtractive manufacturing: 3D printing and milling as respective examples. With additional sensing and closed loop control, or real time optimisation, CNC is also able to adapt for material imperfections and machine wear to achieve higher quality and consistency.

Development in forming automation has not followed suit due to a dependence on part specific tooling - the need for complete moulds in many processes like deep drawing or a complete series of custom profiled rolls for profiled rolling. Consequently, most forming processes remain largely open loop or even human controlled, relying on many repetitions to find optimal operating conditions. This may be sufficient for mass produced items but is unable to meet the demand for flexibility or achieve the tightening quality margins.

A successful control system would depend on the understanding of the process encapsulated in a predictive model that is computable in real time or faster. Current design processes, using finite element models, are computationally too slow so many empirical or ad-hoc models are used instead. For example, Orowan's model [Orowan, 1943] for rolling. A selection of these will be described in the following review section, section 2.

Using a more mathematically rigorous approach, we hope to develop faster solutions that are sufficiently accurate for control systems and help to make CNC forming a reality. Such a systematic approach could also provide insight into the underlying dynamics of forming to improve modelling assumptions and inform process design decisions.

Collaborators in *Cambridge University Engineering Department* are experimentally investigating control of a range of processes such as ring rolling and spinning. Ring rolling reduces the thickness of a ring shaped workpiece by rotating through a pair of rolls called the mandrel and work roll. A second pair of rolls, called the axial rolls, can also be used to reduce the height of the workpiece; all these components are labelled in figure 1. Depending on the operation parameters and use of axial rolls, the workpiece diameter or height can be enlarged as the thickness is reduced. The ongoing investigation is to control the aspect ratio of the workpiece as well as applying profiled or controllable rolls to produce cross-sections more complex than rectangles.

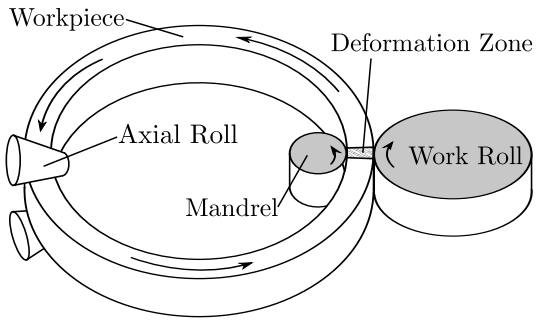

Figure 1: A schematic of a typical ring rolling process indicating the four working tools and the primary deformation zone.

Spinning deforms a circular plate as it is rotated as indicated in figure 2. The roller would make multiple passes along the radial length of the workpiece to incrementally deform the workpiece towards the mandrel that constitutes the final shape. The mandrel is necessary as the workpiece must be pressed firmly onto it to prevent spring back. The current investigation is to replace the mandrel with additional rollers. If tool paths for these rollers can be developed that compensates for spring back and avoids wrinkling or tearing then each unique product shape would not require the production of a mandrel.

There is also a project to construct an experimental flat-sheet rolling machine; much like ring rolling, sheet rolling passes a flat sheet through a pair of rolls to reduce its thickness. The machine is being

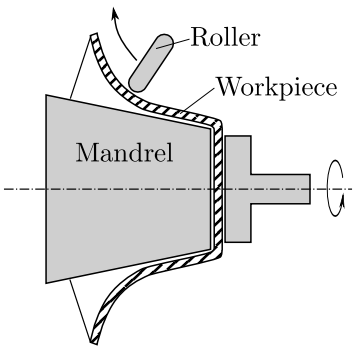

Figure 2: A cross-sectional schematic of a conventional spinning process indicating the workpiece being deformed onto the mandrel as it is rotated.

designed to also apply bending moments on the sheet moving into and out of the roll gap and heat the strip as it is rolled. The ultimate goal is to be able to control the metallurgical properties of the workpiece.

To support the research to be performed with this machine, and as a means of developing an understanding of the field by building on existing literature, enquiry thus far has focused on sheet rolling.

1.1 A primer to rolling

Rolling is the process of reducing the thickness of a flat metal sheet by passing it through a gap between two rolls. Rolling is performed in many different regimes but is generally classed into hot and cold rolling. Hot rolling occurs above the metals recrystallisation point to prevent work hardening. This process is used in rough rolling to reduce large workpieces, such as cast ingots, in to a size appropriate for subsequent stages of manufacture. Some finished products produced with hot rolling are thick sheet metal, I-beams, vehicle frames, building materials and other items with simple cross-sections. Cold rolling occurs below the metals recrystallisation point. Work hardening is therefore a by-product and can be as much as a 20% increase in strength with a 50% thickness reduction. With this work hardening limiting reduction, and a better surface finish than hot rolling, cold rolling typically occurs in the last rolling passes of a workpiece. Cold rolling workpieces are therefore much thinner. Typical products include metal furniture, computer hardware, metal drums and thinner sheet metal.

Although some processes require equipment modifications such as four-high cold rolling mills, functionally, rolling consists of material passing through two turning rolls that reduce the thickness of the material. Figure 3 is a diagram of this idealised process.

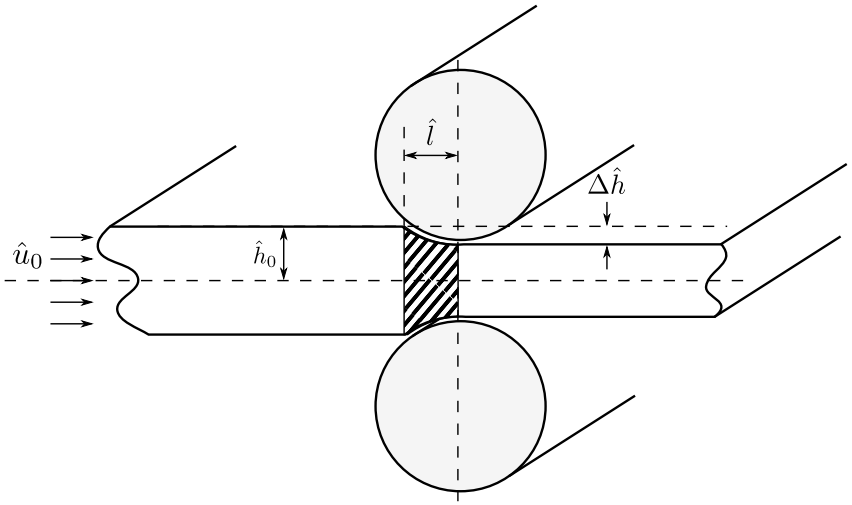

Figure 3: A cross-sectional schematic of rolling indicating the relevant dimensions.

At this point it is worth introducing relevant terminology and geometry. The roll half thickness, $\hat{h}_0$; roll radius, $\hat{R}$; and entrance velocity, $\hat{u}_0$ are all marked in the figure. The roll bite is the region between

the two rolls where the plastic deformation occurs. It is shaded in the figure with the roll bite length marked as $\hat{l}$. The amount the workpiece thickness is reduced is the half gauge, $\Delta\hat{h}$, which is distinct from reduction, which is the fractional change in the workpiece thickness, $r = \Delta\hat{h}/\hat{h}_0$. This distinction will not be of great importance here as these become equivalent after non-dimensionalisation.

Variables denoted with a hat, like those listed, are taken to be dimensional. This is a convention used throughout.

Some key features of the rolling process include the neutral point, pressure hill and coupling between the roll velocities, workpiece velocity and end forces.

Firstly, the rolls of a rolling mill will rotate at some fixed speed so the surface velocity is constant. Considering conservation of mass, it is clear that the material of the workpiece moves faster as it passes through the roll gap. A corollary of these two facts is the existence of a neutral point: a point where the material of the workpiece travels at the same speed as the roll. This is depicted in figure 4 and marked as $\hat{x}_n$.

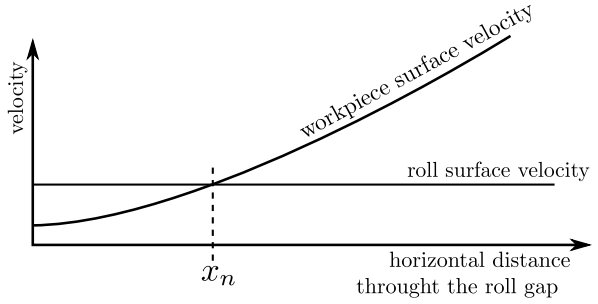

Figure 4: A characteristic plot of the tangential boundary velocity of the workpiece and surface velocity of a roll throughout the roll gap.

The unequal roll and workpiece surface velocity will result in material slipping along the contact faces and hence friction acts to squeeze the workpiece towards the neutral point. This compression builds pressure from both ends to a maximum at the neutral point. This phenomenon is referred to as the pressure hill. It is established by experiment and borne out in all rolling models presented in the literature.

The position of the neutral point will vary depending on the end forces of the workpiece. Extrusion can be considered a special case, where the stationary rolls or extrusion die means the neutral point moves past the roll bite entrance. As the friction of the rolls do not drive the workpiece, a large external pressure is required on the inlet. Drawing would be another special case, similar to extrusion, except that a tension on the outlet replaces the compression force. More generally, the rolls rotate and hence the neutral point exists somewhere in the roll gap so that a combination of end forces and friction act to deform the sheet. In situations such as multiple rolling mills operating in parallel, these end forces may be tension or compression and could work against the flow of material requiring a larger driving force from the rolls.

2 Review of Rolling Literature

Modelling of rolling began in early twentieth century Germany with notable publications including Siebel [1924], Siebel and Pomp [1927], Karman [1925] and Nadai [1931]. These all present variations of a slab model: a model that determines the roll pressure and shear by applying a force balance to each vertical element of the workpiece. This process assumes little through thickness variation of internal stresses and neglects internal shear. Some experimental results may support the validity of this assumption, however, there is no rigorous basis for it and its application in a wide set of regimes is largely unsupported. Despite this, slab models are still being developed and extended to new areas: areas such as asymmetric rolling where shear is likely to become more significant. This will be returned to below.

The next major contribution came from Orowan [1943] in which an approximate model is presented that incorporates shear. Horizontal and vertical force balances are closed by assuming that, locally, the solution can be approximated by Nadai's compressing wedge solution [Nadai, 1931]. This is achieved by considering the section of material contained within the two lines $A - A'$ and $B - B'$ in figure 5. Assuming this region is in dynamic equilibrium then the forces on the dashed lines must equal those on

the solid lines. Then deforming $A - A'$ to be the circumference of a circle perpendicularly intersecting the rolls and $B - B'$ to be a wedge the Nadai [1931] solution can be applied. Applying a wedge solution to this section closes the force balance for each slab of material.

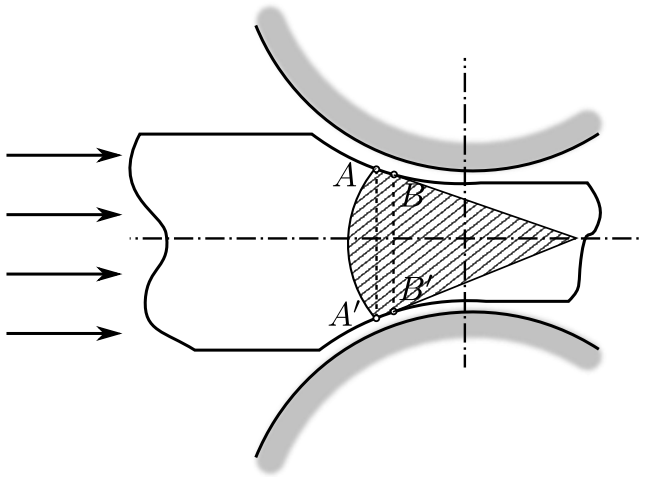

Figure 5: Diagram indicating the approximation of an elemental slab, $A - A' - B', B$, in rolling to a compressing wedge solution (shaded) used by Orowan to close the horizontal and vertical force balances.

Despite Orowan's claims to eliminate ad-hoc assumptions from the analysis, the validity of this assumption is unsubstantiated for two reasons. Firstly, the approximation of the region to a wedge has not been established in any way and, secondly, the compressing wedge solution, although exact, can only be found for material moving toward the wedge apex limiting its correctness to the inlet side of the neutral point. Despite these inaccuracies, this solution has been generally adopted as a benchmark and is widely used by industry, although with empirically fitted parameters.

Some developments since then include Orowan and Pascoe [1946], Bland and Ford [1948b] and Bland and Ford [1948a] which extend Orowan's original work in areas such as incorporating tensions or simplifying the calculation process with additional assumptions.

Slip-line theory has also been utilised in two publications: Alexander [1955] and Collins [1969]. These develop sticking and slipping models respectively although the latter is limited to a qualitative investigation due to the complexity of the fields. Two additional slip-line methods for asymmetric rolling are discussed below in section 2.2.

Hartley et al. [1989] provides the first review of rolling which predominantly covers these classical models as well as experimentation and some early finite element simulation.

Many numerical studies have been performed since they began in 1972 with Alexander [1972]. Notably, Venter and Abd-Rabbo [1980] and Venter and Adb-Rabbo [1980] develop numerical implementations of the Orowan [1943] solution. Finite element simulations have since become very popular and several reviews exist including Montmitonnet and Buessler [1991] and Montmitonnet [2006], in which 34 and 25 publications of finte element have been reviewed respectively. It is, in fact, included as an example problem in the commercial finite element package, *ABAQUS*, 'Example Problems Manual' [Dassault Systemes, 2012]. This ubiquity is a result of the analytical models failing to generalise to a range of materials. Despite this, processing remains slow, too slow for control. The quantitative knowledge from these investigations is also difficult to transfer; the process of constructing and solving these simulations is often repeated in independent studies for nearly identical set-ups.

2.1 Asymptotic Methods

More recently, asymptotic methods have been applied to solve a complete set of governing equations in the limit of a small aspect ratio: thin sheets and large rolls. It was first utilised in metal forming, specifically conical extrusion, in 1987 by Johnson. Having transferred these techniques from modelling creep in glaciers, he considers the pseudo-steady-state conical extrusion of a power-law rate hardening elasto-plastic with Coulomb friction. The asymptotic limit used is quite elegant in that it considers

deviation from a 'plug-like' flow making the solution valid for either low friction or shallow dies. One or both of these assumptions form the basis of all following asymptotic methods in forming. One other publication could be found that examines solid metal extrusion with asymptotics, Govindarajan and Aravas [1991], and it considers shallow die extrusion before adding metal porosity.

Johnson is a named author on numerous publications that apply the same techniques to sheet rolling. The first of these is Smet and Johnson [1989], followed three years later by Johnson and Smelser [1992]. The former applies an almost identical process to that in Johnson [1987] with the further neglection of elasticity. The major distinctions from extrusion are the roll geometry and direction of friction as discussed in section 1.1: opposite direction either side of the neutral point. The latter of the two publications makes a number of simplifications to the former to progress further to a closed form solution; a rigid-plastic material with yield stress as an arbitrary function is used and the magnitude of surface friction is assumed to be a constant fraction of the yield stress.

Although yielding single integral solutions, these assumptions may fail to accurately capture the physics of the problem, particularly the friction model. This motivated a similar formulation in Domanti and McElwain [1995], who re-introduces the more commonly used Coulomb friction, while assuming the ratio of maximum pressure to yield stress is large and the reduction is small. The first of these requires compressive end conditions and the latter, due to the coupling between reduction, roll bite length and sheet thickness, restricts the valid geometry considerably.

Finally, the most comprehensive two-dimensional formulation to date is presented in Cherukuri et al. [1997]. Using a relative-slip friction model and strain-rate dependent constitutive equations, the governing equations are solved to ODEs, assuming only a small aspect ratio. This is repeated for small, medium and large friction then again with no-slip conditions.

Asymptotic approaches to three dimensional effects and spread are considered in Johnson [1991] and Domanti et al. [1994]. The former has a rare comparison to finite element simulations and experimental results. Asymptotic analysis has also been used for stability analysis of 'chatter' in Johnson [1994a]; a multiple scales analysis of work roll heat transfer in Johnson and Keanini [1998]; and a model for roller deformation in Langlands and McElwain [2002]. A review of modelling methods applied to rolling is presented in Domanti and McElwain [1998] although no comparison of results is made.

2.2 Asymmetric Rolling

Asymmetric rolling, when intentional, exploits unequal drive, friction or roll geometry to reduce total force and torque, improve surface finish or improve strain hardening. The challenge, however, is that asymmetry generally induces undesirable curvature.

Experimentation has been used to quantify roll force and torque for a range of geometries and materials [Siebel, 1941, Sachs and Klinger, 1947]. A variety of techniques have also been used to investigate other properties such as contact stress distributions and workpiece curvature [Johnson and Needham, 1966, Buxton and Browning, 1972, Ghobrial, 1989].

Analytical work has included a range of solutions. Most commonly, slab models are modified [Chekmarev and Nefedov, 1956, Kennedy and Slamar, 1958, Sauer and Pawelski, 1987] which has resulted in incremental development to include greater asymmetry and curvature predictions [Mischke, 1996, Hwang and Tzou, 1996, Salimi and Sassani, 2002]. Alternatives also include the upperbound method [Pan and Sansome, 1982, Kiuchi and Hsiang, 1986] and slipline methods [Dewhurst et al., 1974, Collins and Dewhurst, 1975], both of which are able to predict curvature.

Finite element simulations have also been applied to provide detailed solution information for more general configurations. Most studies focus on curvature prediction and roll force distributions [Shivpuri et al., 1988, Richelsen, 1997, Knight et al., 2005].

Asymptotic analysis has only been applied to asymmetric rolling in Johnson [1994b] where an asymmetric friction and roll speed were considered in a friction factor model: that is the surface shear is equal to a constant factor of the yield stress in shear. Asymmetric friction was investigated by changing the friction coefficient of each roll and asymmetric roll speed was modelled by having two independent neutral points and a region of cross shear between them. Roll geometry was also discussed briefly but dismissed as being incorporated into the friction coefficient. Experimental evidence, showing the direction of curvature in asymmetric rolling is dependent on geometry [Collins and Dewhurst, 1975], suggests this approximation is an oversimplification.

3 Governing Equations

This section presents the relevant governing equations for two dimensional plasticity. Force balances are presented which are then closed with material laws presented in section 3.1. Lastly, boundary conditions including multiple material models are presented in section 3.2

Taking a cross-sectional cut through the roll and workpiece, like figure 3, allows a two dimensional problem to be considered as, span wise deformation is negligible sufficiently far from the edge of the workpiece. This plane strain assumption allows the simplification that $\hat{s}_{xx} = -\hat{s}_{yy}$, which is a condition used in all the analysis presented here.

Considering plane strain, the forces on a two dimensional elemental unit of material can be balanced for,

$$-\frac{\partial \hat{p}}{\partial \hat{x}} + \frac{\partial \hat{s}_{xx}}{\partial \hat{x}} + \frac{\partial \hat{s}_{xy}}{\partial \hat{y}} = 0 \tag{1}$$

$$\text{and} \quad -\frac{\partial \hat{p}}{\partial \hat{y}} + \frac{\partial \hat{s}_{yy}}{\partial \hat{y}} + \frac{\partial \hat{s}_{xy}}{\partial \hat{x}} = 0. \tag{2}$$

where $\hat{p}$ is the pressure and $\hat{s}_{ij}$ is the ij^{th} element of the deviatoric stress tensor.

3.1 Material Laws

At least one more equation is required to close this system and completely determine the state of stress. This will form the description of the material behaviour and typically comprises at least four more equations: material flow rules and a yield condition. Many material models exist to describe a range of physical phenomena or satisfy particular analytical properties so several are presented here.

3.1.1 Perfect Plasticity

The Levy-Mises flow rules,

$$\begin{aligned} \frac{\partial \hat{u}}{\partial \hat{x}} &= \hat{\lambda}\hat{s}_{xx}, \\ \frac{\partial \hat{v}}{\partial \hat{y}} &= \hat{\lambda}\hat{s}_{yy} \\ \text{and} \quad \frac{\partial \hat{u}}{\partial \hat{y}} + \frac{\partial \hat{v}}{\partial \hat{x}} &= 2\hat{\lambda}\hat{s}_{xy} \end{aligned} \tag{3}$$

where $\hat{\lambda}$ is the time differential of the flow parameter and $(\hat{u}, \hat{v})$ is the velocity vector, are very simple in so far as they are the associative flow rules of the von Mises yield condition,

$$\hat{s}_{xx}^2 + \hat{s}_{yy}^2 + 2\hat{s}_{xy}^2 = 2\hat{k}^2 \tag{4}$$

where $\hat{k}$ is the yield stress in shear taken to be a constant for perfect plasticity.

The flow rate parameter, $\hat{\lambda}$, is introduced to ensure both material compatibility and the yield condition can be satisfied. It effectively determines the magnitude of plastic deformation while the stress components determine the direction.

It is assumed that the entire roll bite is undergoing plastic deformation so has reached yield, hence the equality in equation (4).

This model describes a rigid perfectly-plastic material with an elliptical yield surface. This is commonly used as the yield surface to describe metals as well as being continuous, making it analytically easier to work with.

3.1.2 Strain-Rate Power Law Hardening

The von-Mises yield condition can be modified to incorporate hardening of several types. Strain-rate power law hardening is achieved by making the yield stress depend on the rate of flow, $\hat{\lambda}$. Defining $\hat{\lambda} = \hat{\Omega}^{n-1}$ then setting $\hat{k} = \hat{\lambda}^{1-n}$ leaves the flow rules as

$$\frac{\partial \hat{u}}{\partial \hat{x}} = \hat{\Omega}^{n-1}\hat{s}_{xx},$$
$$\frac{\partial \hat{v}}{\partial \hat{x}} = \hat{\Omega}^{n-1}\hat{s}_{yy}$$
$$\text{and} \quad \frac{\partial \hat{u}}{\partial \hat{y}} + \frac{d\hat{v}}{d\hat{x}} = 2\hat{\Omega}^{n-1}\hat{s}_{xx}, \tag{5}$$

and the yield condition as

$$\hat{s}_{xx}^2 + \hat{s}_{yy}^2 + 2\hat{s}_{xy}^2 = 2\hat{\Omega}^2. \tag{6}$$

Strain-rate hardening increases the materials resistance to deformation as deformation occurs more quickly. This is usually considered a reasonably accurate model for metals and, as it is still an associative flow rule of the von Mises yield condition, is still analytically simple to work with.

3.1.3 Other Material Models

By making $\hat{k}$ a function of any number of variables many types of hardening are possible. Work hardening is one example that depends on the strain path of each particle of material where the material typically hardens as it is deformed more. Another example is temperature dependence as many materials, particularly metals, soften with heat.

There also exists kinematic, or more generally anisotropic, hardening. This is where the material hardens, or softens, in a given direction due to directional stresses. Kinematic hardening describes the yield surface translating in the stress space where anisotropic hardening could allow the material to harden independently in each direction.

Associative flow rules can also be derived for most yield conditions, such as the Tresca yield condition although this particular flow rule is unnamed. There also exist non-associative flow rules in which there is no specific relation between the flow rule and the yield condition.

Finally, the introduction of elastic deformation could be incorporated as either an elasto-plastic flow rule or by allowing the material to fall below the yield stress.

3.2 Boundary Conditions

Four boundary conditions exist in the rolling problem: two stress conditions and two velocity conditions. There is one each along the roll surface and another integral condition at exit and entrance of the roll gap.

Assuming rigid body motion outside of the roll gap the volume influx is

$$\int_{\hat{h}_0}^{\hat{h}_0} \hat{u}_0 dy = 2\hat{h}_0\hat{u}_0.$$

Considering incompressibility this flux must be constant through every vertical cross section hence

$$2\hat{h}_0\hat{u}_0 = \int_{\hat{h_b}(\hat{x})}^{\hat{h_t}(\hat{x})} \hat{u}(\hat{x},\hat{y})d\hat{y}. \tag{7}$$

Still applying incomressibility, the velocity on the roll surface is attained from considering a no penetration condition,

$$\hat{v}(\hat{x},\hat{h}_t(\hat{x})) = \hat{u}(\hat{x},\hat{h}_t(\hat{x}))\frac{d\hat{h}_t}{d\hat{x}}. \tag{8}$$

This ensures the velocity on the roll surface is tangential to the roll surface.

Accounting for possible horizontal forces on the workpiece outside of the roll gap,

$$\hat{F}_{\text{in}} = \int_{\hat{h}_b(0)}^{\hat{h}_t(0)} \hat{\sigma}_{xx}d\hat{y},$$
$$\text{and} \quad \hat{F}_{\text{out}} = \int_{\hat{h}_b(\hat{l}}^{\hat{h}_t(\hat{l})} \hat{\sigma}_{xx}d\hat{y}. \tag{9}$$

where $\hat{\sigma}_{xx}$ and $\hat{\sigma}_{yy}$ are the total longitudinal stresses or $\hat{\sigma}_{xx} = -\hat{p} + \hat{s_{xx}}$ and similarly for the vertical stress.

Stress conditions on the roll surfaces are found by considering horizontal and vertical equilibrium on a boundary volume element. A detailed derivation is given in appendix A with the final condition found to be

$$\hat{s}_{xy} = \hat{\tau}_t \left(1 + \left(\frac{d\hat{h}_t}{d\hat{x}}\right)^2\right) - 2\hat{s}_{xx}\frac{d\hat{h}_t}{d\hat{x}} + \hat{s}_{xy}\left(\frac{d\hat{h}_t}{d\hat{x}}\right)^2. \tag{10}$$

where $\hat{\tau}_t$ is the interfacial friction.

This is closed with a friction model; like material models a large range of friction models exist and a few are presented here.

3.2.1 Coulomb Friction

Coulomb friction is a widely used friction model and has been applied to static and slipping friction, although coefficient values are often very different. It is developed on the assumption that the friction force is proportional to the normal pressure,

$$\hat{\boldsymbol{\tau}} = \mu\hat{\boldsymbol{\sigma}} \cdot \mathbf{n}\frac{\Delta\hat{\mathbf{u}}}{|\Delta\hat{\mathbf{u}}|} \tag{11}$$

where $\Delta\mathbf{u}$ is the relative slip velocity of the plastic material past the surface, μ is a constant friction coefficient and $\mathbf{n}$ is the unit normal vector to the contact surface.

3.2.2 Relative-Slip

Relative-slip friction is specifically a slipping model as it defines the friction force as proportional to the velocity difference between the surfaces in contact,

$$\hat{\boldsymbol{\tau}} = \hat{\kappa}\Delta\hat{\mathbf{u}} \tag{12}$$

where $\hat{\kappa}$ is a constant friction coefficient.

3.2.3 Other Friction Models

An assortment of other models have been identified in literature.

Friction Factor

The friction factor model appears to be a significant simplification, often used to make a problem more tractable. It assumes that the friction force is constant at some fraction of the yield stress,

$$\hat{\boldsymbol{\tau}} = c\hat{k}\frac{\Delta\hat{\mathbf{u}}}{|\Delta\hat{\mathbf{u}}|} \tag{13}$$

where c is a constant friction factor.

No-slip

The no-slip condition assumes that the friction is sufficiently high to ensure the materials stick. In terms of velocities it is

$$\hat{\mathbf{u}} = \hat{\mathbf{U}} \tag{14}$$

where $\hat{\mathbf{U}}$ is the roll velocity. For rigid perfectly-plastic, and other materials, this will leave the stresses undetermined and so the associated stress condition is a friction factor model where $c = 1$.

Transitional Models

As the traction exceeds the material yield, the friction will transition from a slipping to a no-slip model. Some solutions are able to capture this behaviour, such as Orowan [1943].

Similarly, some models try to combine Coulomb and relative-slip friction with some transition region. Experimentally there is evidence that supports these models as Coulomb friction performs well for static and low relative velocity differences where relative-slip is more accurate for higher relative velocities.

One such example of this is a model developed in Karabin and Smelser [1990]:

$$\hat{\boldsymbol{\tau}} = |\hat{\boldsymbol{\tau}}| \frac{\Delta \hat{\mathbf{u}}}{|\Delta \hat{\mathbf{u}}|}$$
$$\text{where} \quad |\hat{\boldsymbol{\tau}}| = \min\left(\mu\psi\hat{s}, \hat{k}\right)$$
$$\text{and} \quad \psi = \min\left(\frac{|\Delta \mathbf{u}|}{\Delta_v}, 1\right) \tag{15}$$

where μ and Δ_v are both constants. Note that ψ is defined with a nondimensionalised slip velocity. Effectively this formulation will behave like relative slip at low slip speeds, when $\psi < 1$, then transition to a Coulomb model at higher speeds, when $\psi = 1$ makes $|\hat{\boldsymbol{\tau}}| = \mu\hat{s}$, before transitioning to a sticking model to not exceed the yield condition, $|\hat{\boldsymbol{\tau}}| = \hat{k}$.

4 Symmetric Rolling

Two models are presented in this section: rigid perfectly-plastic with Coulomb and relative-slip friction. Neither have been explicitly presented in literature, however, they are only a new combination of assumptions from the four publications of asymptotic modelling of two-dimensional symmetric rolling discussed in section 2.1.

Although this work is in part filling in the gaps left in literature some interesting insights arise about limitations of certain assumptions. This suggests the most simple models lack sufficient phenomena to be completely consistent.

This section begins by non-dimensionalising the equations presented in the previous section with some discussion about the choice of scaling. Specifically, the force balance equations at the beginning of section 3, the material rules in section 3.1.1 and both Coulomb friction in section 3.2.1 and relative-slip friction in section 3.2.2. One of several choices of scaling is selected to present the solution method. This is completed for a general friction model before Coulomb and relative-slip models are each applied. Some results from these models are compared with finite element simulations and then an alternative scaling with a discussion of their limitations which may go some way to explain the selection of models used in the existing literature.

4.1 Non-dimensionalisation and Generalised Solution

It is first worth noting again, dimensional quantities are denoted with a hat and non-dimensional quantities without.

Define δ as the ratio of vertical to horizontal characteristic length scales, chosen as input half thickness and roll bite length respectively so $\delta = \hat{h}_0/\hat{l}$. This is the small parameter that featured often in previous asymptotic studies of rolling and extrusion. It separates the directional derivatives, essential to making analytical progress.

This parameter indicates at a number of scalings. Obviously scaling $\hat{x}$ by the roll gap length, $\hat{l}$, and $\hat{y}$ by the input half thickness, $\hat{h}_0$. The horizontal velocity can be scaled by some characteristic velocity, $\hat{u}_0$, taken here as the input velocity. This can can ultimately be chosen to satisfy the roller speeds if the problem specifies these instead. The vertical velocity is taken to balance the horizontal velocity in the no-penetration boundary conditions, hence scaling $\hat{v} = v\delta\hat{u}_0$.

The stress scalings are less obvious as, despite some constraints, there remains some freedom in relative sizes. Begin by defining characteristic shear, deviatoric longitudinal stress and pressure, $\hat{\tau}_0$, $\hat{s}_0$ and $\hat{p}_0$ respectively. Now consider the yield condition. This suggests the larger (or both if similar magnitude) of the deviatoric and shear stresses could be scaled by the yield stress $\hat{k}$.

Balancing the derivatives in each direction of the horizontal equilibrium requires $\hat{\tau}_0 = \delta\max\left(\hat{s}_0, \hat{p}_0\right)$ although solving in the case where $\hat{s}_0 > \hat{p}_0$ leads to an inconsistency: pressure jumping an order. This indicates that the more correct balance is between pressure and shear stress hence $\hat{\tau}_0 = \delta\hat{p}_0$. Finally, define $\bar{\beta}$ as the ratio of characteristic deviatoric shear to longitudinal stresses, $\hat{\tau}_0/\hat{s}_0$, and it is possible then to enumerate three possibilities based on the magnitude of $\bar{\beta}$.
In ascending order, if $\bar{\beta} = O(\delta)$ then

$$\hat{s}_0 = \hat{k}, \qquad \hat{\tau}_0 = \bar{\beta}\hat{k} \quad \text{and} \qquad \hat{p}_0 = \frac{\bar{\beta}}{\delta}\hat{k}.$$

If $\bar{\beta} = O(1)$ then

$$\hat{s}_0 = \hat{k}, \qquad \hat{\tau}_0 = \bar{\beta}\hat{k} \quad \text{and} \qquad \hat{p}_0 = \frac{\bar{\beta}}{\delta}\hat{k}.$$

But, if $\bar{\beta} = O(\delta^{-1})$ then

$$\hat{s}_0 = \frac{\hat{k}}{\bar{\beta}}, \qquad \hat{\tau}_0 = \hat{k} \quad \text{and} \qquad \hat{p}_0 = \frac{\hat{k}}{\delta}.$$

As it may be obvious by its definition, $\bar{\beta}$ is some measure of the size of friction. In its most elegant case it maps to the Coulomb friction coefficient but may depend on other parameters, such as velocities in the relative-slip model. Selections of these regimes have been made implicitly in the previous asymptotic rolling literature. Smet and Johnson [1989], Johnson and Smelser [1992] both use the middle friction regime and Domanti and McElwain [1995] assume the friction is small yet the pressure is large which contradicts these scalings. To achieve this, compressive end conditions are required to raise the pressure in the roll gap - a point not mentioned in the publication. This choice was made explicitly in Cherukuri et al. [1997] where all three were solved in turn.

Not all these regimes provide adequate solutions with certain material or friction models which may explain why some of these earlier publications did not more comprehensively address the issue. The limitation of these models is discussed in greater detail in section 4.5.

The final scaling to decide is the flow rate parameter which is chosen so the horizontal flow equation balances at leading order, hence $\hat{\lambda} = \frac{\hat{u}_0}{\hat{s}_0}\lambda$.

As this solution process becomes both expansive and repetitive only the case where $\bar{\beta} = O(\delta)$ will be presented in full. Other regimes will be illustrated through comparison to this solution.

For convenience, let $\beta = \bar{\beta}/\delta = O(1)$ so the governing equations for force equilibrium are

$$-\beta\frac{\partial p}{\partial x} + \frac{\partial s_{xx}}{\partial x} + \beta\frac{\partial s_{xy}}{\partial y} = 0, \tag{16}$$

$$\text{and} \quad -\beta\frac{\partial p}{\partial y} + \frac{\partial s_{yy}}{\partial y} + \beta\delta^2\frac{\partial s_{xy}}{\partial x} = 0; \tag{17}$$

for flow are,

$$\frac{\partial u}{\partial x} = \lambda s_{xx}, \tag{18}$$

$$\frac{\partial v}{\partial y} = \lambda s_{yy}, \tag{19}$$

$$\text{and} \quad \frac{\partial u}{\partial y} + \delta^2\frac{\partial v}{\partial x} = 2\delta^2\beta\lambda s_{xy}; \tag{20}$$

for incompressibility, or equally in this case plane strain, is

$$\frac{\partial u}{\partial x} + \frac{\partial v}{\partial y} = 0; \tag{21}$$

and for yield is,

$$s_{xx}^2 + s_{yy}^2 + 2\delta^2\beta^2 s_{xy}^2 = 2,$$

or

$$s_{xx}^2 + \delta^2\beta^2 s_{xy}^2 = 1 \tag{22}$$

when plane strain is considered. Also boundary conditions for velocity are

$$v(x,h) = u(x,h)\frac{dh}{dx}$$

$$v(x,0) = 0, \tag{23}$$

$$\text{and} \quad 1 = \int_0^{h(x)} u(x,y)dy; \tag{24}$$

and for stress are

$$s_{xy}(x,h) = \tau(x)\left(1+\delta^2\left(\frac{dh}{dx}\right)^2\right) - \frac{2}{\beta}\frac{dh}{dx}s_{yy}(x,h(x)) + \delta^2 s_{xy}(x,h(x))\left(\frac{dh}{dx}\right)^2,$$

$$s_{xy}(x,0) = 0, \tag{25}$$

$$\hat{F}_{\text{in}}\frac{1}{2\hat{h}_0\hat{k}} = \int_0^{h(0)} \sigma_{xx}(0,y)dy,$$

$$\text{and} \quad \hat{F}_{\text{out}}\frac{1}{2\hat{h}_0\hat{k}} = \int_0^{h(1)} \sigma_{xx}(1,y)dy \tag{26}$$

where we approximate the roll as a parabola so that

$$h(x) = 1 - r(2x - x^2)$$
$$\text{and} \quad \frac{dh}{dx} = -2r(1-x).$$

Taking all parameters as $O(1)$, except $\delta \ll 1$, these equations describe pseudo-steady state rigid perfect-plastic, small aspect ratio, low friction plane-strain rolling.

4.1.1 Expansion in δ

Taking the aspect ratio, δ, as the small parameter, each dependant variable, v_x, v_y, S_{xx}, S_{yy}, S_{xy}, p and λ, is expanded in typical asymptotic style.

$$a(x,y) = a^{(0)}(x,y) + \delta a^{(1)}(x,y) + \delta^2 a^{(2)}(x,y) + ...$$

Substitute these expansions into the governing equations and boundary conditions. Then, assuming δ is sufficiently small that each power of δ is disparate and can be considered orthogonal to one another, group like terms produces a series of, what is hoped to be, tractable equations that can be progressively solved for an increasingly accurate solution. The equations will be presented at the beginning of each relevant section.

4.1.2 Considering $O(1)$ Terms

To recap, the leading order equations are

$$-\beta\frac{\partial p^{(0)}}{\partial x} + \frac{\partial {s_{xx}}^{(0)}}{\partial x} + \beta\frac{\partial {s_{xy}}^{(0)}}{\partial y} = 0, \tag{27}$$

$$-\beta\frac{\partial p^{(0)}}{\partial y} - \frac{\partial {s_{xx}}^{(0)}}{\partial y} = 0, \tag{28}$$

$$\frac{\partial u^{(0)}}{\partial x} = \lambda^{(0)}{s_{xx}}^{(0)}, \tag{29}$$

$$\frac{\partial v^{(0)}}{\partial x} = -\lambda^{(0)}{s_{xx}}^{(0)}, \tag{30}$$

$$\frac{\partial u^{(0)}}{\partial y} = 0, \tag{31}$$

$$\frac{\partial u^{(0)}}{\partial x} + \frac{\partial v^{(0)}}{\partial y} = 0, \tag{32}$$

$${s_{xx}}^{(0)2} = 1, \tag{33}$$

$$s_{xy}{}^{(0)}(x,h(x)) = s_{xy}{}^{(0)}(x,h(x)) + \frac{2}{\beta}\frac{dh}{dx}s_{xx}{}^{(0)}(x,h(x)),$$

$$s_{xy}{}^{(0)}(x,0) = 0, \tag{34}$$

$$\int_0^1 -\beta p^{(0)}(0,y) + s_{xx}{}^{(0)}(0,y)dy = \frac{\hat{F}_{\text{in}}}{2\hat{k}\hat{h}_0},$$

$$\int_0^{h(1)} -\beta p^{(0)}(1,y) + s_{xx}{}^{(0)}(1,y)dy = \frac{\hat{F}_{\text{out}}}{2\hat{k}\hat{h}_0}, \tag{35}$$

$$1 = \int_0^{h(x)} u^{(0)}(x,y)dy, \tag{36}$$

$$v^{(0)}(x,h(x)) = \frac{dh}{dx}u^{(0)}(x,h(x)),$$

$$\text{and} \quad v^{(0)}(x,0) = 0. \tag{37}$$

Begin by determining the leading order velocities; integrating equation (31) shows that leading order horizontal velocity is a function of x only. Using the conservation of mass argument, equation (36), readily produces the result

$$u^{(0)} = \frac{1}{h(x)}. \tag{38}$$

Substituting this into equation (32) gives an equation for the leading order vertical velocity. After integration and the application of the boundary conditions, equation (37), the solution is found to be

$$v^{(0)} = \frac{y}{h(x)^2}\frac{dh}{dx}. \tag{39}$$

Now the longitudinal deviatoric stresses are determined from equation (33) which rearranges to

$$s_{xx}{}^{(0)} = -s_{yy}{}^{(0)} = 1 \tag{40}$$

where the sign has been chosen assuming the compression from the rolls is greater than the end conditions. This is required to not violate the scalings chosen between pressure and longitudinal stresses.

Diverting momentarily from stresses, the flow rate parameter can now be solved by rearranging equation (18) for

$$\lambda^{(0)} = \frac{1}{h(x)^2}\frac{dh}{dx}. \tag{41}$$

Returning now to the shear stress and pressure, these remaining variables are coupled through the horizontal force balance, equation (27), and the choice of friction condition. Fortunately, substituting equation (40) into the vertical force balance, equation (28), reveals that the leading order pressure is independent of y. This, with equation (40) substituted again, simplifies equation (27) to a pressure derivative balanced by a shear derivative. Integrating in y between the boundary conditions and substituting equation (25) gives an equation for pressure,

$$\frac{dp^{(0)}}{dx} = \frac{s_{xy}{}^{(0)}(x,h(x))}{h(x)} = \frac{\tau^{(0)}(x)}{h(x)} + \frac{2}{\beta h(x)}\frac{dh}{dx}. \tag{42}$$

This will either be an integral equation for relative-slip friction or an ordinary differential equation for Coulomb friction or something less tractable for more complex boundary conditions.

The constants of integration here provide the flexibility to determine where the neutral point occurs. Depending on the friction model applied this may couple the workpiece velocity scaling, $\hat{u}_0$, and the roll velocities as well as the end tensions and roll torque.

Either by inspection or by an integrating equation (27) in y it can be determined that leading order shear is linear in y. With both boundary conditions, equation (25), this is sufficient to determine

$$s_{xy}{}^{(0)} = y\frac{s_{xy}{}^{(0)}(x,h(x))}{h(x)} = y\left(\frac{\tau^{(0)}(x)}{h(x)} + \frac{2}{\beta h(x)}\frac{dh}{dx}\right). \tag{43}$$

4.1.3 Considering $O(\delta)$ Terms

Similarly, the equations for the first order corrections are

$$-\beta\frac{\partial p^{(1)}}{\partial x} + \frac{\partial {s_{xx}}^{(1)}}{\partial x} + \beta\frac{\partial {s_{xy}}^{(1)}}{\partial y} = 0, \tag{44}$$

$$-\beta\frac{\partial p^{(1)}}{\partial y} - \frac{\partial {s_{xx}}^{(1)}}{\partial y} = 0, \tag{45}$$

$$\frac{\partial u^{(1)}}{\partial x} = \lambda^{(1)}{s_{xx}}^{(0)} + \lambda^{(0)}{s_{xx}}^{(1)}, \tag{46}$$

$$\frac{\partial v^{(1)}}{\partial x} = -\lambda^{(1)}{s_{xx}}^{(0)} - \lambda^{(0)}{s_{xx}}^{(1)}, \tag{47}$$

$$\frac{\partial u^{(1)}}{\partial y} = 0, \tag{48}$$

$$\frac{\partial u^{(1)}}{\partial x} + \frac{\partial v^{(1)}}{\partial y} = 0, \tag{49}$$

$$2{s_{xx}}^{(1)}{s_{xx}}^{(0)} = 0, \tag{50}$$

$$\begin{aligned} {s_{xy}}^{(1)}(x,h(x)) &= {s_{xy}}^{(1)}(x,h(x)) \\ {s_{xy}}^{(1)}(x,0) &= 0, \end{aligned} \tag{51}$$

$$\int_0^1 -\beta p^{(1)}(0,y) + {s_{xx}}^{(1)}(0,y)dy = 0,$$

$$\int_0^{h(1)} -\beta p^{(1)}(1,y) + {s_{xx}}^{(1)}(1,y)dy = 0, \tag{52}$$

$$0 = \int_0^{h(x)} u^{(1)}(x,y)dy, \tag{53}$$

$$\begin{aligned} v^{(1)}(x,h(x)) &= \frac{dh}{dx}u^{(1)}(x,h(x)), \\ \text{and} \quad v^{(1)}(x,0) &= 0. \end{aligned} \tag{54}$$

Repeating this process for the next order leads to the first order velocities, flow rate parameter and longitudinal deviatoric stresses all to be identically zero. Both the first order pressure and shear stress will also be zero unless there is some first order frictional effect, as

$$\frac{dp^{(1)}}{dx} = \frac{{s_{xy}}^{(1)}(x,h(x))}{h(x)} = \frac{\tau^{(1)}(x)}{h(x)} \tag{55}$$

$$\text{and} \quad {s_{xy}}^{(1)} = y\frac{{s_{xy}}^{(1)}(x,h(x))}{h(x)} = y\frac{\tau^{(1)}(x)}{h(x)}. \tag{56}$$

4.1.4 Considering $O(\delta^2)$ Terms

The second order corrections are the next set of non-trivial solutions although they increase considerably in complexity due to the forcing terms of the leading order. Due to this complexity they do not provide much additional insight into the system except for introducing y dependence in the pressure, longitudinal stress and horizontal velocity terms as well as quadratic y dependence in shear and vertical velocity.

A second order solution has been provided in appendix B, however, this is for the asymmetric Coulomb friction case which will be presented to leading order in the next section.

4.2 Applying Friction Models

Having now determined the equations for the velocities, stresses and flow rate parameter given an arbitrary friction model, it is now straightforward to substitute friction models to compare their behaviour and limitations.

4.2.1 Coulomb

From appendix A, the friction boundary conditions to the first two orders are

$$s_{xy}{}^{(0)}(x,h(x)) = \frac{\Delta\mathbf{u}}{|\Delta\mathbf{u}|}\frac{\mu}{\bar{\beta}}\frac{\bar{\beta}}{\delta}p^{(0)} + \frac{\mu}{\bar{\beta}}\frac{\Delta\mathbf{u}}{|\Delta\mathbf{u}|}s_{xx}{}^{(0)} + \frac{2\delta}{\bar{\beta}}s_{xx}{}^{(0)}\frac{dh(x)}{dx} \tag{57}$$

$$\text{and} \quad s_{xy}{}^{(1)}(x,h(x)) = 0. \tag{58}$$

Taking $\bar{\beta} = \mu$ so $\beta = \frac{\mu}{\delta}$ leaves the ordinary differential equation from equation (42)

$$\frac{dp^{(0)}}{dx} \mp \frac{\beta}{h(x)}p^{(0)}(x) = \left(\frac{2}{\beta}\frac{dh}{dx} \pm 1\right)\frac{s_{xx}{}^{(0)}}{h(x)} \tag{59}$$

where the top sign is applied upstream of the neutral point and the bottom sign applied downstream. This can be solved in each piecewise region for

$$p^{(0)} = e^{\int \pm\beta\frac{1}{h(x)}dx}\left(c_0 + \int e^{\int \mp\beta\frac{1}{h(x)}dx}\frac{2}{\beta h(x)}\frac{dh(x)}{dx}dx\right) - \frac{1}{\beta}.$$

where c_0 is constant in each piecewise region. Assuming the parabolic form for the rolls, this can be simplified to

$$p^{(0)} = \frac{4r}{\beta}\left(\frac{x-1-\sqrt{\frac{r-1}{r}}}{x-1+\sqrt{\frac{r-1}{r}}}\right)^{\frac{\pm\beta}{2}\sqrt{\frac{r}{r-1}}}(c_0' - K) - \frac{1}{\beta}.$$

where

$$K = \int\left(\frac{x-1+\sqrt{\frac{r-1}{r}}}{x-1-\sqrt{\frac{r-1}{r}}}\right)^{\frac{\pm\beta}{2}\sqrt{\frac{r}{r-1}}}\frac{4r\,(1-x)}{\beta\,(1-r\,(2x-x^2))}dx.$$

K can be solved by using partial fractions in terms of hypergeometric functions,

$$\begin{aligned}K = {} & \pm\frac{\eta-2}{\beta}\left(-\frac{\eta+\xi}{2\eta}\right)^{\frac{\pm\beta}{2\eta}}{}_2F_1\left(\frac{\pm\beta}{2\eta},\frac{\pm\beta}{2\eta};\frac{\pm\beta}{2\eta}+1;\frac{\eta+\xi}{2\eta}\right)\\ & + \frac{\eta+2}{2\eta\pm\beta}\left(-\frac{\eta+\xi}{2\eta}\right)^{\frac{\pm\beta}{2\eta}+1}{}_2F_1\left(\frac{\pm\beta}{2\eta}+1,\frac{\pm\beta}{2\eta}+1;\frac{\pm\beta}{2\eta}+2;\frac{\eta+\xi}{2\eta}\right)\end{aligned}$$

where $\xi = x-1$ and $\eta = \sqrt{\frac{r-1}{r}}$.

It is also possible to solve for the constants of integration,

$$c_0' = \left(\frac{\xi-\eta}{\xi+\eta}\right)^{\frac{\mp\beta}{2\eta}}\frac{\beta}{4r}\left(p^{(0)}(x) + \frac{1}{\beta}\right) - K$$

where

$$p^{(0)}(0) = \left(1 - \frac{\hat{F}_{\text{in}}}{2\hat{h}_0\hat{k}}\right)$$

$$\text{or} \quad p^{(0)}(1) = \left(1 - \frac{\hat{F}_{\text{out}}}{2\hat{h}_0\hat{k}}\right).$$

This result substitutes easily to complete the leading order shear stress

$$s_{xy}{}^{(0)} = \frac{y}{h(x)}\left(s_{xx}{}^{(0)}\left(2\frac{dh}{dx} \pm 1\right) \pm \beta p^{(0)}(x)\right) = \frac{y}{1-r\,(2x-x^2)}\left(\pm\beta p^{(0)}(x) \pm 1 - 4r\,(1-x)\right). \tag{60}$$

As there is no first order correction to the friction force the first order corrections to both pressure and shear stress are found to be zero.

The neutral point is then selected to ensure continuity in horizontal stress, or pressure as s_{xx} trivially satisfies this. The neutral point couples the roll speed and the workpiece entrance velocity. The velocity scaling can therefore be chosen to satisfy either the input velocity or the roll velocity, whichever is specified.

4.2.2 Relative-Slip

Repeat this for the relative-slip friction model, which to the first two orders are

$$s_{xy}{}^{(0)}(x, h(x) = \kappa \frac{U - u^{(0)}}{h(x)} + \frac{2}{\beta h(x)} \frac{dh}{dx} \tag{61}$$

$$\text{and} \quad s_{xy}{}^{(1)}(x, h(x)) = 0 \tag{62}$$

where U is the roll surface velocity. This would suggest $\beta = \frac{\hat{\kappa} \Delta \hat{u}_0}{\delta \hat{k}}$.

With this, the pressure can be solved with a single integration,

$$p^{(0)} = \int \kappa \frac{U - u^{(0)}}{h(x)} + \frac{2}{\beta h(x)} \frac{dh}{dx} \, \mathrm{d}x, \tag{63}$$

which can be reduced to closed form with the rolls taking parabolic form,

$$p^{(0)} = \frac{\kappa}{2} (U - r) \sqrt{\frac{r}{r-1}} \log \left(\frac{x - 1 - \sqrt{\frac{r-1}{r}}}{x - 1 + \sqrt{\frac{r-1}{r}}} \right) + \left(\kappa r + \frac{2}{\beta} \right) \log \left(1 - r \left(2x - x^2 \right) \right)$$

The shear is, again, an easy substitution for the closed form solution,

$$s_{xy}{}^{(0)} = y \left(\kappa \frac{U - u^{(0)}}{\Delta U h(x)} + \frac{2}{\beta h(x)} \frac{dh}{dx} \right). \tag{64}$$

4.3 Results

Figure 6 presents the roll pressure and shear stress distribution for an example case with both Coulomb and relative-slip friction. The example case is of a 2mm workpiece with 100MPa yield stress in shear. Rolls of 200mm radius reduce the workpiece by 30% giving $\delta = 0.09$. The friction coefficients, μ and $\hat{\kappa}$, are both set to 0.1.

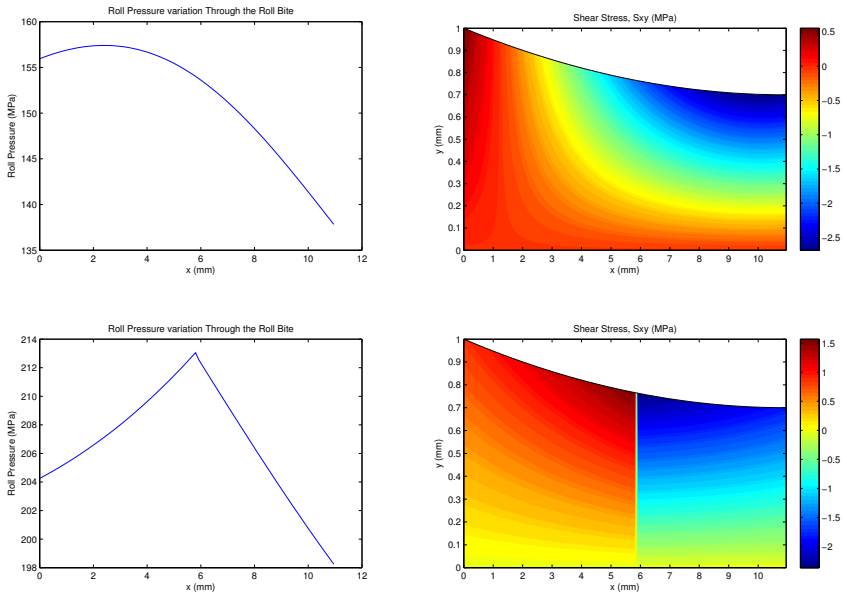

Figure 6: Plots showing the roll pressure (left) and shear stress distribution (right) for low magnitude relative-slip (top) and Coulomb friction (bottom) asymptotic models.

It can be seen that both models exhibit a pressure hill, however, the similarities end there. The friction models produce radically differing shear distributions which each suffer from a discontinuity. The relative-slip model produces the greatest shear at either end of the roll gap before losing contact

with the roll and becoming a stress free boundary. The Coulomb friction produces the highest shear at the pressure peak which coincides with the change in direction of slip at the boundary, and hence the sudden change in direction of shear.

A finite element simulation was completed for comparison using the commercial *ABAQUS* package, figure 7. A larger δ was used with workpiece thickness of 3mm, roll bite length of 5mm and a reduction of 15%, due to computational limitations as δ approaches zero, discussed below. The yield stress was the same, however, elasticity is included in *ABAQUS*; to minimise its effect, the Young's modulus was increased to 69GPa. A mass scaling of 1000 was also used.

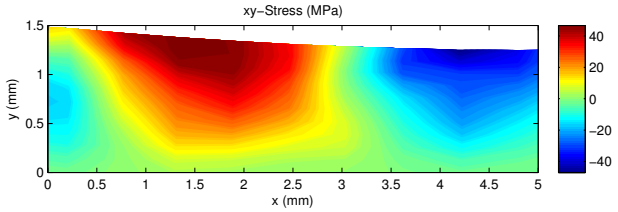

Figure 7: Shear stress distribution generated from an *ABAQUS* simulation.

This solution has neither of these discontinuities as the shear drops to zero around the neutral points as well as falling at either end of the roll gap. The friction model implemented in *ABAQUS*, and used in this simulation, is Coulomb friction. This explains the ends of the roll bite but not near the neutral point where the solution looks closer to the relative-slip case. Despite the appearance, this will be the result of very different mechanics; it is likely the material falls below yield near the neutral point. An elastic plug like this has been referred to in several publications such as Collins [1969]. This is a phenomena these asymptotic models will not capture as the material is artificially held at the yield condition.

All three models have zero shear along the centreline due to the symmetry of the problem.

The results of the asymptotic models are compared with a slab model and Orowan's model, identified in section 2, as well as some unsuccessful finite element simulations. The geometry and material properties were the same as the asymptotic models above, except for the friction coefficient and workpiece thickness which were varied as specified in the x-axes.

Firstly, the finite element simulations have clearly not converged. These are here to illustrate that the *ABAQUS* solver performs poorly as δ is reduced. Finer meshes are required to prevent the elements becoming elongated with the roll gap, however, more elements slow computational time until it becomes unpractical. To gain numerical results in this limit, a bespoke solver, that solves a scaled set of equations, is required. This is mentioned again in the next section and discussed further in section 8 as future work.

All four analytical methods produce similar trends as δ is varied. The asymptotic models fall between the slab model and Orowan's solution for the roll force but predict a slightly higher roll torque. This is unsurprising as the resolved internal shear will contribute to the roll torque.

As the friction coefficient is varied the relative-slip model performs similarly to Orowan's solution. The Coulomb friction model is closer to the slab model in roll force but is much greater than all others in roll torque. This failing of the Coulomb friction model is unsurprising as it clearly exceeds the assumption of small friction used during its derivation. It is more surprising that the relative-slip model continues to perform well as the same assumption was made. This may be a decreasing material speed allowing the model to keep the magnitude of friction within reasonable limits. This will require further investigation.

4.4 Medium Friction

The solution process above can be repeated with $\bar{\beta} = O(1)$. This produces the same results at leading order except for the longitudinal deviatoric stress which, from equation (22), takes the form

$$s_{xx}{}^{(0)} = -s_{yy}{}^{(0)} = \sqrt{1 - \bar{\beta}^2 s_{xy}{}^{(0)2}}. \tag{65}$$

These equations can be solved for either friction model and produce results that are similar to those of small friction. The longitudinal deviatoric stress is no longer homogeneous, however, the remaining variables are only altered by a scaling.

Figure 9 shows the roll pressure and shear stress distribution using the same parameters as the equivalent figures in the previous section except for addition of end tensions and the increase of the

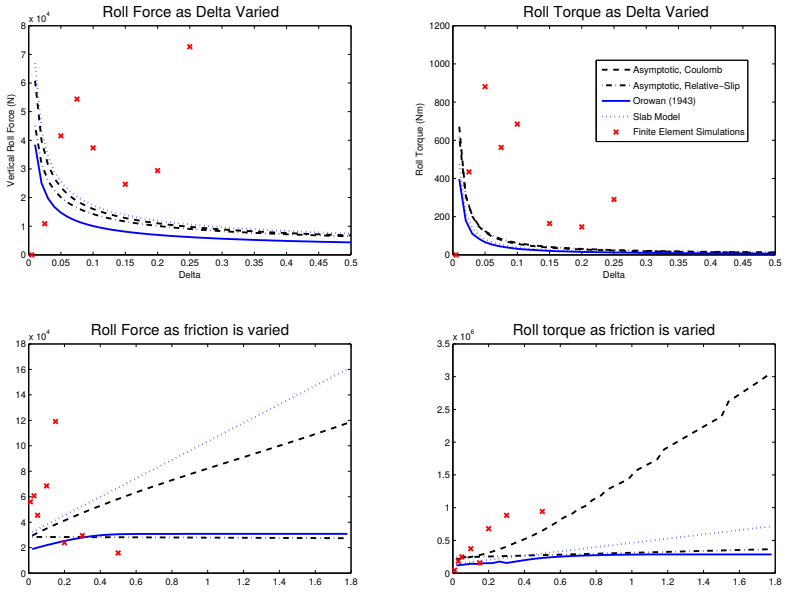

Figure 8: A comparison of roll force (left) and torque (right) between Coulomb friction models from finite element simulation with *ABAQUS* (crosses), a slab model (dotted line), Orowan's solution (solid line) and asymptotic models (dashed line) as the roll gap ratio (top) and friction coefficient (bottom) were varied.

friction coefficient to 0.9. Compressive end forces were introduced to satisfy the scaling requirements of

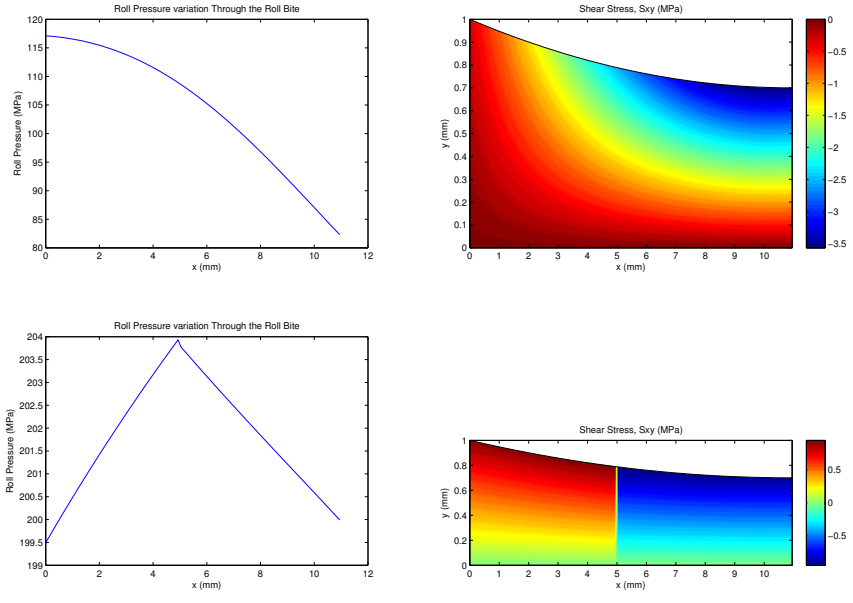

Figure 9: Roll pressure and shear stress distribution for relative slip (top) and Coulomb friction (bottom) asymptotic models with friction coefficients of order one.

the Coulomb friction case. When friction and pressure are coupled, like Coulomb friction, the small order of friction works satisfactorily, however, the larger friction can not be satisfied without larger pressure which does not exist at the roll bite ends unless compression conditions are applied. This is an inherent problem with the scaling and leads to the pressure dropping an order without the correct, compression,

boundary conditions. This is also the case with Domanti et al. [1994] although it is not discussed there.

Once this has been accounted for, there is little change in form from the small friction case, although, it is a little surprising that the increase in pressure through the roll gap is less than in the low friction case.

4.5 Discussion

The solution depends heavily on the model and magnitude of friction but many pitfalls exist with different combinations of these. Two successful regimes were presented in sections 4.2.1 and 4.2.2, however, the latter of these was found to have severe limitations as the magnitude of friction was increased, as discussed in section 4.4.

As friction is increased transitioning to sticking, or a no-slip condition, must also be considered. This was circumvented by Cherukuri et al. [1997] who used a strain-rate hardening model that would simply harden instead of sticking. It should be addressed, however, especially for applications such as hot rolling.

To understand the complete behaviour of each combination of material model and friction model, a solution will need to be found each regime of friction: $\beta = O(\delta)$, $\beta = O(1)$ and $\beta = O(\delta^{-1})$. This is clearly a non-trivial task due to the difficulties outlined above.

The common model choices are laid out with publications that address each combination in table 1.

Material Model	Coulomb Friction	Relative-Slip	No-Slip
Perfectly-Plastic	Domanti et al. [1994] Section 4.2.1	Section 4.2.2	
Strain-Rate Dependent	Section 6	Cherukuri et al. [1997]	Cherukuri et al. [1997]
Strain Dependent	Smet and Johnson [1989]		

Table 1: Table of work performed on each material and friction models.

Completing this table is unlikely to produce a completely physical description of what is going on as transitional models, elasticity and entrance regions could be required to recreate results similar to the finite element simulations. However, with a sufficient understanding of the behaviour of each model it is likely an adequate approximation could be found for most applications.

5 Weakly Asymmetric Friction, Geometry and Roll Speeds

In this section it is no longer assumed that the rolling process is symmetric; variation may exist between the top and bottom rolls in friction, size and drive speed. It is, however, assumed that for each of these characteristics the ratio between the top and bottom roll remains $O(1)$. The approach to finding a solution is identical to the previous section, except that integrals are taken between the top and bottom roll surfaces instead of using the symmetry plane. This requires a second set of boundary conditions: a vertical reflection with the second set of roll parameters.

The governing equations and scalings used are the same as those in section 4.1 for small $\bar{\beta}$ so this section proceeds to the solution, section 5.2, after discussing some points about geometry, section 5.1. The section concludes with some comparison to finite element simulations and discussion of the quality of these models in section 5.3.

5.1 Workpiece Alignment

Firstly, we take the rolls to be vertically aligned. It is then assumed that the workpiece feeds into the roll gap in such a way that the initial contact with each roll, tri-junctions or points A and B in figure 10, are vertically aligned. The effect of plastic deformation will also ensure that the workpiece leaves the roll gap at the centre line of the rolls, where the roll bite is thinnest.

Asymmetry, in general, will induce a bending moment at either end of the roll bite, bending the workpiece around either roll and violating the previous assumptions. This effect, however, is assumed to be negligible for this analysis. This could become the limiting effect of this model but is a common

assumption within the literature [Chekmarev and Nefedov, 1956, Kennedy and Slamar, 1958, Sauer and Pawelski, 1987].

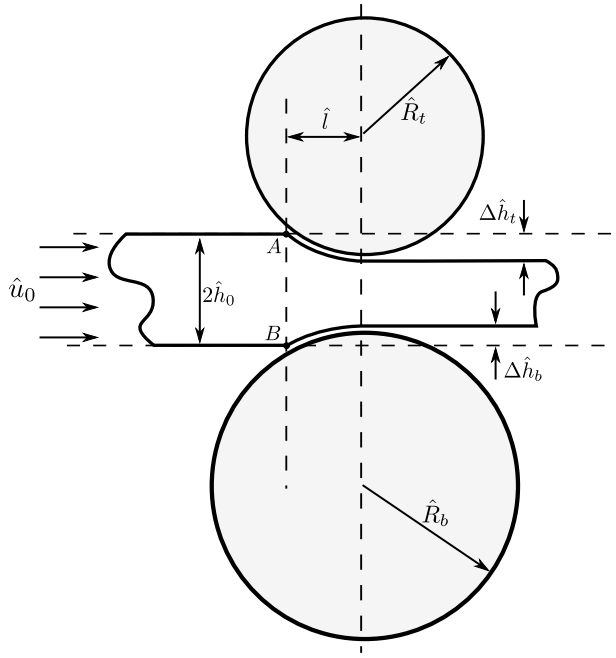

Figure 10: Illustration of the asymmetric roll configuration. Note the vertical alignment of tri-junctions, A and B, on the inlet. The same alignment for the outlet is satisfied by vertically aligning the rolls.

Defining roll sizes, R_t and R_b; total reduction, $2r = \frac{\Delta\hat{h}_t + \Delta\hat{h}_b}{2\hat{h}_0}$; and workpiece thickness $2\hat{h}_0$ is sufficient to geometrically determine the system. All these parameters are marked in figure 10. It can then be calculated that the top and bottom reductions are given by

$$r_t = \frac{4r\hat{R}_b - 4r^2}{2\hat{R}_t + 2\hat{R}_b - 4r}$$
$$\text{and} \quad r_b = \frac{4r\hat{R}_t - 4r^2}{2\hat{R}_t + 2\hat{R}_b - 4r} = 2r - r_t$$

and the roll bite length is

$$\hat{l}^2 = \min\left(2\hat{R}_t\hat{h}_0 r_t - \hat{h}_0^2 r_t^2, 2\hat{R}_b\hat{h}_0 r_b - \hat{h}_0^2 r_b^2\right).$$

We shall define $\Delta h = h_t(x) - h_b(x)$ for convenience. This should not be ambiguous as the roll gauge is not referred to again.

5.2 Solution

Derivations of the friction boundary conditions are included in appendix A but for reference the results are

$$s_{xy}(x, h_t(x)) = \tau_t(x)\left(1 + \delta^2\left(\frac{dh_t}{dx}\right)^2\right) - \frac{2}{\beta}\frac{dh_t}{dx}s_{yy}(x, h_t(x)) + \delta^2 s_{xy}(x, h_t(x))\left(\frac{dh_t}{dx}\right)^2$$
$$\text{and} \quad s_{xy}(x, h_b(x)) = \tau_b(x)\left(1 + \delta^2\left(\frac{dh_b}{dx}\right)^2\right) - \frac{2}{\beta}\frac{dh_b}{dx}s_{yy}(x, h_b(x)) + \delta^2 s_{xy}(x, h_b(x))\left(\frac{dh_b}{dx}\right)^2. \quad (66)$$

In addition the integrals of the other boundary conditions from section 4.1 are extended to both rolls giving

$$\begin{aligned}
\hat{F}_{\text{in}}\frac{1}{\hat{h}_0\hat{k}} &= \int_{h_b(0)}^{h_t(0)} \sigma_{xx}(0,y)dy, \\
\hat{F}_{\text{out}}\frac{1}{\hat{h}_0\hat{k}} &= \int_{h_b(1)}^{h_t(1)} \sigma_{xx}(1,y)dy, \qquad (67)\\
v(x,h_t) &= \delta u(x,h_t)\frac{dh_t}{dx}, \\
v(x,h_b) &= \delta u(x,h_b)\frac{dh_b}{dx}, \qquad (68)\\
\text{and} \quad 2 &= \int_{h_b(x)}^{h_t(x)} u(x,y)dy. \qquad (69)
\end{aligned}$$

Using the equations from section 4 and the new boundary conditions the solution is re-derived using the process in sections 4.2.1 and 4.2.2.

The velocities are found to be

$$u^{(0)} = \frac{2}{\Delta h} \qquad (70)$$

$$\text{and} \quad v^{(0)} = \frac{2}{\Delta h^2}\left(h_t\frac{dh_b}{dx} - h_b\frac{dh_t}{dx} + y\frac{d\Delta h}{dx}\right). \qquad (71)$$

Longitudinal deviatoric stress required no integration and so is found to be the same.

The flow rate parameter is now

$$\lambda^{(0)} = \frac{2}{\Delta h^2}\frac{d\Delta h}{dx}. \qquad (72)$$

This leaves the pressure and shear stress which can be solved in their general form as

$${s_{xy}}^{(0)} = \frac{s_{xy}^{(0)}(x,h_t(x)) - s_{xy}^{(0)}(x,h_b(x))}{h_t(x) - h_b(x)}y + \frac{h_t(x){s_{xy}}^{(0)}(x,h_b(x)) - h_b(x){s_{xy}}^{(0)}(x,h_t(x))}{h_t(x) - h_b(x)}. \qquad (73)$$

and

$$\frac{dp^{(0)}}{dx} = \frac{{s_{xy}}^{(0)}(x,h_t(x)) - {s_{xy}}^{(0)}(x,h_b(x))}{h_t(x) - h_b(x)} \qquad (74)$$

where the constant of integration are to be solved, as discussed before, using the end tensions.

5.2.1 Coulomb Friction

Once again, taken from appendix A, the friction boundaries are

$$\begin{aligned}
{s_{xy}}^{(0)}(x,h_t(x)) &= \frac{\Delta\mathbf{u}}{|\Delta\mathbf{u}|}\frac{\mu}{\bar{\beta}}\frac{\bar{\beta}}{\delta}p^{(0)}(x,h_t(x)) + \frac{\mu}{\bar{\beta}}\frac{\Delta\mathbf{u}}{|\Delta\mathbf{u}|}{s_{xx}}^{(0)}(x,h_t(x)) + \frac{2\delta}{\bar{\beta}}{s_{xx}}^{(0)}(x,h_t(x))\frac{dh_t(x)}{dx}, \\
{s_{xy}}^{(1)}(x,h_t(x)) &= 0, \\
{s_{xy}}^{(0)}(x,h_b(x)) &= \frac{\Delta\mathbf{u}}{|\Delta\mathbf{u}|}\frac{\mu}{\bar{\beta}}\frac{\bar{\beta}}{\delta}p^{(0)}(x,h_b(x)) + \frac{\mu}{\bar{\beta}}\frac{\Delta\mathbf{u}}{|\Delta\mathbf{u}|}{s_{xx}}^{(0)}(x,h_b(x)) + \frac{2\delta}{\bar{\beta}}{s_{xx}}^{(0)}(x,h_b(x))\frac{dh_b(x)}{dx} \\
\text{and} \quad {s_{xy}}^{(1)}(x,h_b(x)) &= 0. \qquad (75)
\end{aligned}$$

By defining functions that encapsulate the non-dimensionalised friction coefficient and the direction friction is acting,

$$\gamma_t = \begin{cases} \frac{\mu_t}{\bar{\beta}} & : x < x_{nt} \\ -\frac{\mu_t}{\bar{\beta}} & : x > x_{nt} \end{cases}, \qquad \gamma_b = \begin{cases} -\frac{\mu_b}{\bar{\beta}} & : x < x_{nb} \\ \frac{\mu_b}{\bar{\beta}} & : x > x_{nb} \end{cases},$$

where x_{nt} is the neutral point on the top roller and x_{nb} is the equivalent on the bottom roller, the effects of friction are more easily interpreted. Already it can be seen that two neutral points introduce a third region known as the region of cross shear.

Define $\Delta\gamma = \gamma_t - \gamma_b$ which is a generalisation of the dual sign in section 4.2.1 that can hold a third state for the cross shear region. Similar to the symmetric case, the differential equation for pressure is solved in each region where $\Delta\gamma$ is constant and then each solution is matched at the intersections.

The solution for the two outer regions are found using the end forces as initial conditions. The middle solution must then be matched to these outer two solutions. The intersections determine the neutral points which in turn determine the roll velocities. The middle solution must therefore satisfy the specified roll speed ratio such that $\frac{u^{(0)}(x_{Nt})}{u^{(0)}(x_{Nb})} = \frac{U_t}{U_b}$. This coupling is illustrated in figure 11. The absolute velocities are then satisfied by changing the velocity scaling of the solution, $\hat{u}_0$.

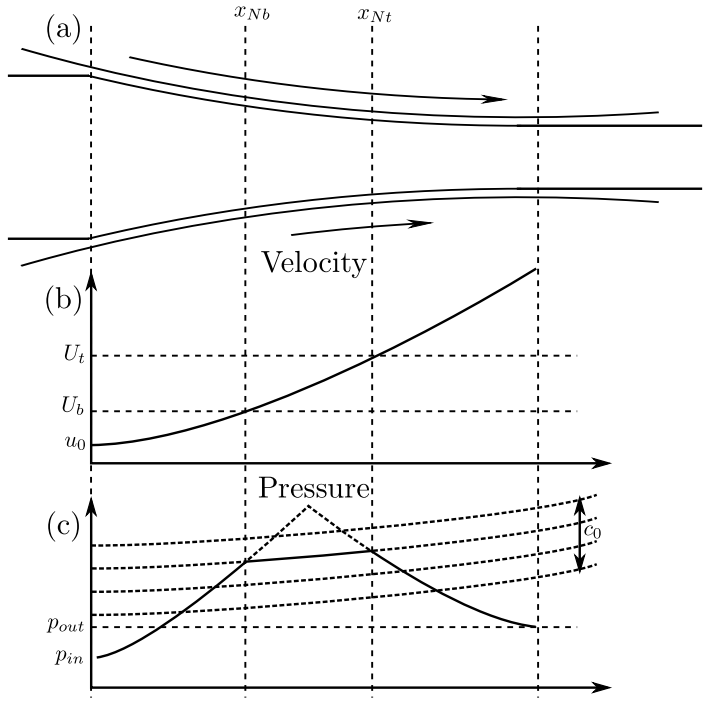

Figure 11: Figure showing the roll gap (a), characteristic form of pressure through the roll gap (b) and the characteristic form of velocity through the roll gap (c). The top and bottom neutral point are marked and indicated with vertical dotted lines show the relation between physical location of the neutral points, roll velocities, and regions of the pressure differential equaiton.

Substituting these boundary conditions equation (75), into the general solution, equation (74) produces the differential equation, where there is an additional term over the symmetric case,

$$\frac{\partial p^{(0)}}{\partial x} - \beta p^{(0)} \frac{\Delta\gamma}{\Delta h} = \frac{\Delta\gamma}{\Delta h} + \frac{2}{\beta \Delta h} \frac{d\Delta h}{dx}. \tag{76}$$

Assuming $\Delta\gamma$ is constant over the considered region

$$p^{(0)} = \frac{2}{\beta} \log(\Delta h) + c_0$$

if $\Delta\gamma = 0$, and

$$p^{(0)} = e^{\int \beta \frac{\Delta\gamma}{\Delta h} dx} \left(c_0 + \int e^{-\int \beta \frac{\Delta\gamma}{\Delta h} dx} \frac{2}{\beta \Delta h} \frac{d\Delta h}{dx} dx \right) - \frac{1}{\beta}.$$

if $\Delta\gamma \neq 0$. After substituting parabolic rollers, this second result simplifies to

$$p^{(0)} = \left(-\frac{x - 1 + \sqrt{\frac{r-1}{r}}}{x - 1 - \sqrt{\frac{r-1}{r}}} \right)^{\beta \frac{\Delta\gamma}{2} \sqrt{\frac{r}{r-1}}} \left(c_0 + \int \left(\frac{x - 1 + \sqrt{\frac{r-1}{r}}}{x - 1 - \sqrt{\frac{r-1}{r}}} \right)^{\beta \frac{\Delta\gamma}{2} \sqrt{\frac{r}{r-1}}} \frac{2r(x-1)}{\beta\left(1 - r(2x - x^2)\right)} dx \right) - \frac{1}{\beta}.$$

A closed form of this integral can be produced in terms of hyper-geometric and Appell hyper-geometric functions.

Now the shear stress can be determined by substituting this result into

$$s_{xy}{}^{(0)}(x,y) = -\frac{\beta p^{(0)}(x)+1}{\Delta h}\left(\Delta\gamma y + (\gamma_t(x)h_b(x) - \gamma_b(x)h_t(x))\right). \tag{77}$$

Like the symmetric case, there is no contribution from the first order correction.

$O(\delta^2)$ corrections increase in complexity, again, due to the forcing from the leading order. For this reason they have been relegated to appendix B.

5.2.2 Relative-Slip Friction

The tractions with relative-slip friction are

$$\begin{aligned}
\tau_t &= \frac{U_t - u_s(x,h_t(x))}{\Delta U} = \frac{U_t - u(x,h_t(x))\left(1+\frac{1}{2}\delta^2\frac{d^2h}{dx^2}+O(\delta^3)\right)}{U_t-u_0} \\
\text{and}\quad \tau_b &= \kappa\frac{U_b - u_s(x,h_b(x))}{\Delta U} = -\kappa\frac{U_b - u(x,h_b(x))\left(1+\frac{1}{2}\delta^2\frac{d^2h}{dx^2}+O(\delta^3)\right)}{U_b-u_0}
\end{aligned}$$

which give the shear conditions as

$$\begin{aligned}
s_{xy}{}^{(0)}(x,h_t(x)) &= \frac{u^{(0)}(x,h_t(x))-U_t}{\Delta U} - \frac{2}{\beta}\frac{dh_t}{dx} = \frac{2-U_t\Delta h}{\Delta h\Delta U} - \frac{2}{\beta}\frac{dh_t}{dx}, \\
s_{xy}{}^{(1)}(x,h_t(x)) &= 0, \\
s_{xy}{}^{(0)}(x,h_b(x)) &= -\kappa\frac{u^{(0)}(x,h_b(x))-U_b}{\Delta U} - \frac{2}{\beta}\frac{dh_b}{dx} = -\kappa\frac{2-U_b\Delta h}{\Delta h\Delta U} - \frac{2}{\beta}\frac{dh_t}{dx}, \\
\text{and}\quad s_{xy}{}^{(1)}(x,h_b(x)) &= 0.
\end{aligned} \tag{78}$$

The pressure term can now be integrated directly for

$$p^{(0)} = \int \frac{2}{\Delta h\Delta U}(1+\kappa) + \frac{1}{\Delta U}(U_t+\kappa U_b) - \frac{2}{\beta}\frac{d\Delta h}{dx}dx. \tag{79}$$

5.3 Results and Discussion

Unsurprisingly, the results of the asymmetric solution are very similar to the symmetric case. Asymmetric friction coefficients and asymmetric roll size have similar effects: moving the line of zero shear toward the roll with less friction or the smaller roll and moving the neutral point in the relative-slip model. This effect is larger from variations in the roll sizes. Roll speeds have a significant effect on neutral points of the Coulomb friction model but this is much less prominent in the relative-slip case.

An example of each of these friction models is provided in figures 12 and 13. This example considers a 2mm sheet with 10% reduction and 100MPa yield stress in shear. All three asymmetries were introduced as illustration. The top roll radius is 210mm with a friction coefficient, μ and $\hat{\kappa}$, of 0.1 and run at 10.2mm per second. The bottom roll radius is 180mm with a friction coefficient of 0.1 and run at 10mm per second. This gave δ as 0.16 which is large but not unreasonably so. Also, no end tension was applied.

The models match reasonably considering the different underlying assumptions. There is also no reason to believe that μ and $\hat{\kappa}$ should be equivalently scaled. Despite this the pressure hills rise to 161MPa and 129MPa respectively and the variation in roll shear are both around 50MPa, although nearly opposite in trend.

Certain features to note include the differences in shear in the cross-shear region. Both have regions of fairly uniform stress except the Coulomb friction case is much more obvious as shear is highest at the centre. This high stress throughout the entire region contrasts with the region of lowest shear in the relative-slip model.

Similarly, the roll shear exhibits a large jump at both neutral points for the Coulomb model, where as the relative-slip model exhibits no visual difference to the symmetric case.

Finally, it is interesting to note that the pressure hills begin to look similar as the tops are flattened on both. This, again, is the result of the region of cross-shear, where the workpiece is no longer being squeezed inwards. Without this frictional force building the pressure, the gradient is dominated by the component of the normal stress on the boundary. This could be interpreted as the resistance due to the geometrical change being exerted on the workpiece.

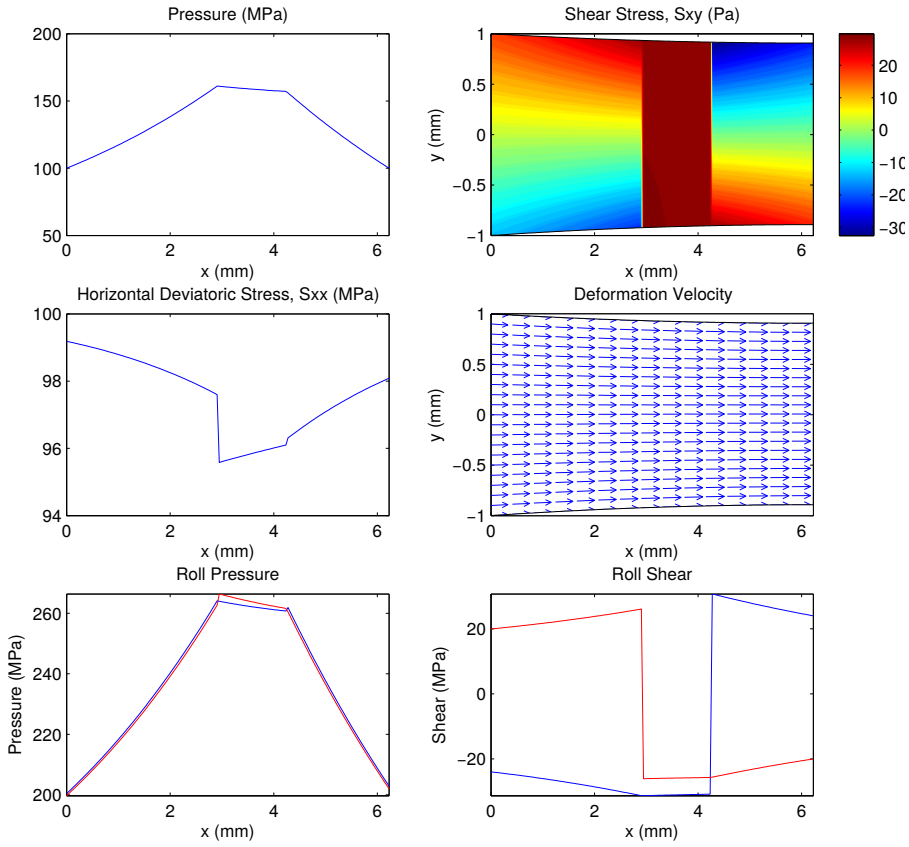

Figure 12: From top left; pressure, shear stress, deviatoric stress, flow map, roll pressure and roll shear for an asymmetric small Coulomb friction asymptotic model.

Figure 14 presents the force and torque for each roll, comparing the Coulomb friction model with finite element simulation results. The symmetric case was a 5mm thick workpiece with 100MPa yield stress in shear undergoing 12% reduction with 2.5m radius rolls, friction coefficient of 0.1 and 1.2m per second surface roll speed. These parameters reduced δ to 0.91 which is more comfortably in the thin-sheet regime. These are particularly large rolls and it is more likely the workpiece would be thinner which would maintain the scaling. The roll size, speed and friction coefficient of the bottom roll was varied while the top roll was unchanged to produce the ratios on the x-axes of the figure.

The trend as each parameter is varied matches well, although deterioration begins with large disparity between roll speeds as the asymptotic results plateau too soon. This behaviour, especially the rapid transition in the roll torque is a consequence of the neutral points shifting and eventually reaching the end of the roll gap, hence the plateau observed in both the numerical and analytical results. These results suggest that the neutral point of the asymptotic solution responds too quickly to the introduced speed asymmetry. This observation is consistent with comparisons to the relative-slip model and may be a consequence of the asymptotic scalings.

While the trends match reasonably well, the magnitude appears to be off-set by a constant factor. This remains unaccounted for but may be the result of additional physics incorporated into the *ABAQUS* simulation. It is intended to develop a numerical simulation of the perfect-plastic equations to determine whether this is the case or whether the discrepancy is a feature of the asymptotics, or even implementation error.

The stepping in the torque results of the asymptotic solutions is believed to be numerical as it did not arise in the implementation of a similar model. Regardless, this must be investigated further by implementing the pressure and shear stress with differing uses of numerical computation - using an ODE solver, numerical integration or hyper-geometric functions.

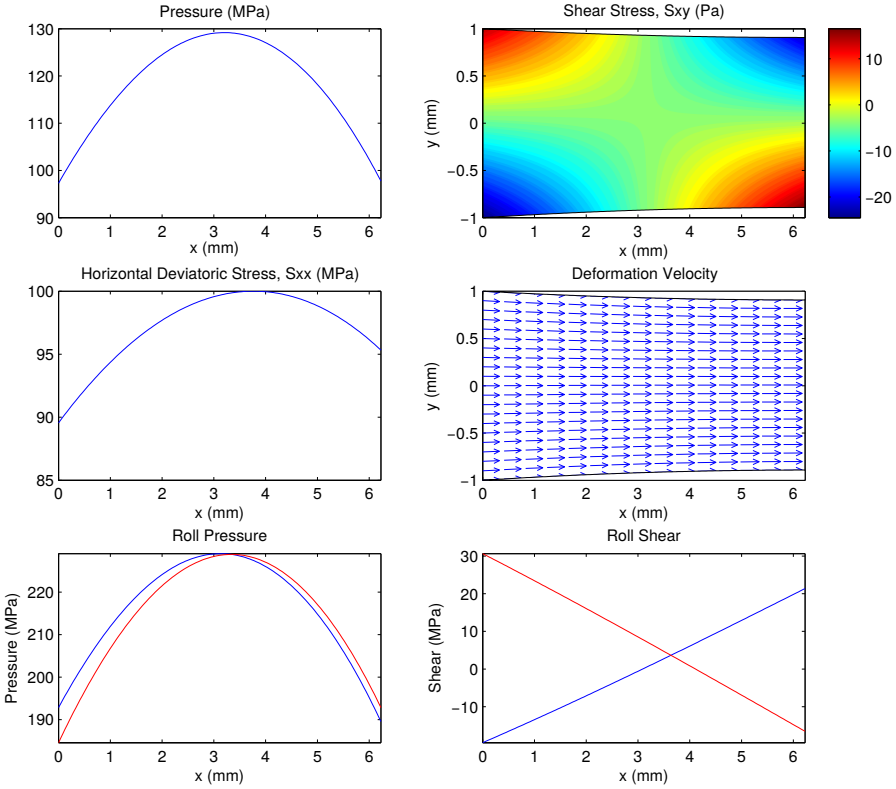

Figure 13: From top left; pressure, shear stress, deviatoric stress, flow map, roll pressure and roll shear for an asymmetric small relative-slip friction asymptotic model.

6 Strain-Rate Power Law Hardening

In this section the perfect-plastic material law will be replaced with a strain-rate power law hardening law as it is more accurate in modelling metals. It is still a Levy-Mises flow rule but derived from a von Mises yield condition with a yield stress that increases with the flow rate parameter. This model is presented in section 3.1.2.

This change only affects the stress solutions compared to the perfect plastic model at leading order. The new stress results then propagate to all other variables at second order adding additional terms to the equations, although not adding considerable complexity to the calculation.

As the relative-slip case can be found in Cherukuri et al. [1997] only the Coulomb friction model solution to first order corrections is presented here.

6.1 Flow and Yield Equations

The governing equations and boundary conditions are identical to those used in the asymmetric case, section 5.2.1 with the exception of the flow laws and yield condition that are replaced with equations (5) and (6). These are non-dimensionalised as

$$\frac{\partial u}{\partial x} = \Omega^{n-1} s_{xx}, \tag{80}$$

$$\frac{\partial v}{\partial y} = \Omega^{n-1} s_{yy}, \tag{81}$$

$$\frac{\partial u}{\partial y} + \delta^2 \frac{\partial v}{\partial x} = 2\beta\delta^2 \Omega^{n-1} s_{xy} \text{and} \quad s_{xx}^2 + \delta^2 \beta^2 s_{xy}^2 = \Omega^2 \tag{82}$$

where $\hat{\Omega}$ is scaled by $\hat{s}_0$ and $\hat{s}_0 = \left(\frac{\hat{u}_0}{\hat{B}\hat{l}}\right)^{\frac{1}{n}}$. Both n and $\hat{B}$ are material parameters.

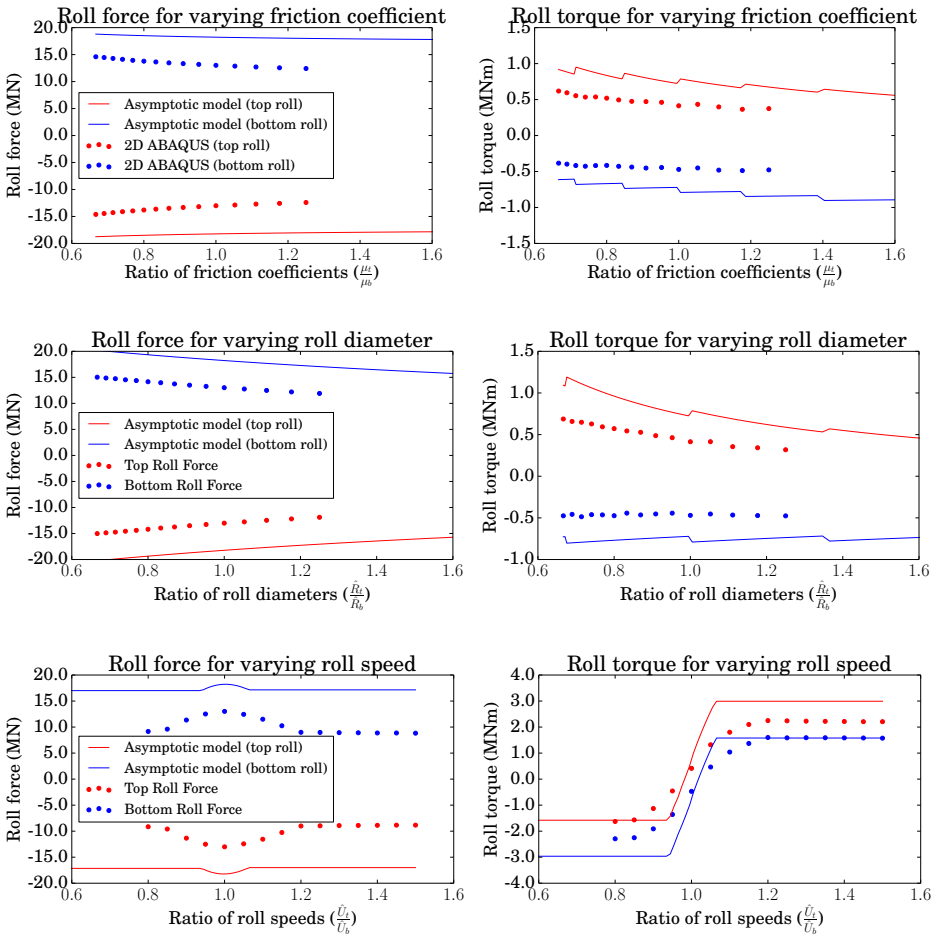

Figure 14: Comparison of roll force (left) and torque (right) between the small Coulomb friction, asymmetric asymptotic model (solid line) and finite element simulations with the commercial package ABAQUS (dots). The extent of asymmetry is varied by changing the bottom rolls friction coefficient (top), diameter (middle) and speed (bottom) ratios.

The hardening effect reduces as n is increased such that this model tends to the perfect plastic model in the limit $n \to \infty$.

6.2 Solution

The leading order solution for velocity remains unchanged from that in section 4.1. The leading order equations that have changed are

$$\frac{\partial u^{(0)}}{\partial x} = \left(\Omega^{(0)}\right)^{n-1} {s_{xx}}^{(0)}, \tag{83}$$

$$\frac{\partial v^{(0)}}{\partial y} = \left(\Omega^{(0)}\right)^{n-1} {s_{yy}}^{(0)}, \tag{84}$$

$$\frac{\partial u^{(0)}}{\partial y} = 0, \tag{85}$$

$${s_{xx}}^{(0)2} = \Omega^{(0)2} \tag{86}$$

The new yield condition, equation (86), gives the condition

$${s_{xx}}^{(0)} = \pm\Omega^{(0)}$$

which means equation (83) is now required to solve for ${s_{xx}}^{(0)}$. With plane strain, this gives

$$ {s_{xx}}^{(0)} = -{s_{yy}}^{(0)} = \left(\frac{\partial u^{(0)}}{\partial x}\right)^{\frac{1}{n}} = \left(\frac{-1}{\Delta h^2}\frac{d\Delta h}{dx}\right)^{\frac{1}{n}} \tag{87} $$

where the sign of $\Omega^{(0)}$ is chosen to make the base of the exponent positive. This could equally be found from equation (84).

Using the same approach as in section 4 and section 5, the horizontal force balance, equation (16), shows $p^{(0)}$ is independent of y which allows the vertical force balance to be integrated with respect to y for

$$ {s_{xy}}^{(0)} = \left(\frac{dp^{(0)}}{dx} - \frac{1}{n\beta}\left(\frac{-2}{\Delta h^2}\frac{d\Delta h}{dx}\right)^{\frac{1}{n}-1}\left(\frac{2}{\Delta h^3}\left(\frac{d\Delta h}{dx}\right)^2 - \frac{1}{\Delta h^2}\frac{d^2\Delta h}{dx^2}\right)\right) y + c_1(x). \tag{88} $$

Applying the friction boundary conditions equation (75), both $c_1(x)$ and the coefficient of y can be solved. The latter produces an ordinary differential equation for pressure,

$$ \frac{dp^{(0)}}{dx} - \frac{\Delta u}{\beta\delta\Delta h}p^{(0)} = \left(\frac{\Delta\mu}{\beta\delta\Delta h} + \frac{4}{\beta\Delta h}\frac{d\Delta h}{dx}\right){s_{xx}}^{(0)} + \frac{1}{n\beta}\left(\frac{-2}{\Delta h^2}\frac{d\Delta h}{dx}\right)^{\frac{1}{n}-1}\left(\frac{2}{\Delta h^3}\left(\frac{d\Delta h}{dx}\right)^2 - \frac{1}{\Delta h^2}\frac{d^2\Delta h}{dx^2}\right), \tag{89} $$

and the former substitutes back for ${s_{xy}}^{(0)}$,

$$ \begin{aligned} {s_{xy}}^{(0)} = &\left(\frac{\Delta u}{\beta\delta\Delta h}p^{(0)} + \left(\frac{\Delta\mu}{\beta\delta\Delta h} + \frac{4}{\beta\Delta h}\frac{d\Delta h}{dx}\right){s_{xx}}^{(0)}\right) y \\ &+ \frac{1}{\beta\Delta h}\left(\frac{h_t\mu_b - h_b\mu_t}{\delta}\left(p^{(0)} + {s_{xx}}^{(0)}\right) + 2\left(h_t\frac{dh_b}{dx} - h_b\frac{dh_t}{dx}\right){s_{xx}}^{(0)}\right). \end{aligned} \tag{90} $$

Like the perfect-plastic case, the first order corrections are identically zero.

7 Clad Sheet Rolling

Another extension to this model is the rolling of clad sheet; that is sheet comprised of two metals bonded together. The asymmetry introduced by the material properties will result in some curvature of the plate and so it is often desireable to counter this through control or machine design.

Like the strain-rate hardening in the previous section, the influence of material properties has no effect on the leading order velocities. The boundary of the two materials can be determined as a free boundary using mass conservation. The stress state will be changed from the asymmetric homogeneous material solution to ensure a lower yield stress in the softer material while balancing normal and tangential forces through the interface of the two materials.

7.1 Formulation

The problem is formulated with Coulomb friction only, for brevity, so is identical to section 5.2.1 with the addition of a free boundary that is the interface of two materials with differing yield stresses. The variables of the second material, taken to be below the interface, will be denoted as capitals, for example the second yield stress is $\hat{K}$ and non-dimensionalised to $K = \frac{\hat{K}}{\hat{k}}$. This would make the yield condition of the second material

$$ S_{xx}^2 + \beta^2\delta^2 S_{xy}^2 = K^2. $$

All other equatons are correct with capitalised variables.

The material interface, $g(x)$, is defined the same way as the roll profiles: distance from the centreline. Velocities of both materials are defined to be equal at the interface,

$$ u(x, g(x)) = U(x, g(x)), \qquad v(x, g(x)) = V(x, g(x)). \tag{91} $$

Similarly, the surface tractions on the interface are balanced,

$$
\begin{aligned}
\beta\tau_s &= \frac{1}{1+\delta^2 g'^2}\left(-2g's_{xx} + \beta s_{xy}\left(1-\delta^2 g'^2\right)\right)\\
&= \frac{1}{1+\delta^2 g'^2}\left(-2g'S_{xx} + \beta S_{xy}\left(1-\delta^2 g'^2\right)\right) = \beta \mathrm{T}_s\\
\text{and}\quad \tau_n &= \beta p\left(1+\delta^2 g'^2\right) + s_{xx}\left(1-\delta^2 g'^2\right) + \delta^2\beta s_{xy} g'\\
&= \beta P\left(1+\delta^2 g'^2\right) + S_{xx}\left(1-\delta^2 g'^2\right) + \delta^2\beta S_{xy} g' = \mathrm{T}_n.
\end{aligned}
\tag{92}
$$

7.2 Solution

As mentioned above, the material parameters have no effect on determining velocity profiles at leading order so, as the material interface ensuers velocity continuity, these remain unchanged from the asymmetric case. The velocity calculations in this case also produce an equation for the material interface,

$$
g^{(0)}(x) = \frac{\Delta h(x)}{2}\left(g(0)-1\right). \tag{93}
$$

The new yield condition produces a longitudinal deviatoric stresses for both materials,

$$
s_{xx} = -s_{yy} = 1 \quad \text{and} \quad S_{xx} = -S_{yy} = K. \tag{94}
$$

This changes the flow rate parameter in the lower half of the material to

$$
\Lambda^{(0)} = \frac{2}{K\Delta h^2}\frac{d\Delta h}{dx}. \tag{95}
$$

The horizontal force balance still shows that leading order pressure is independent of y but the vertical force balance must be integrated and applied between h_b and g then g and h_t. This, with equation (92), gives a system of four equations,

$$
\begin{aligned}
\frac{dp^{(0)}}{dx}h_t(x) + c_0 &= \beta\gamma_t\left(\beta p^{(0)} + {s_{xx}}^{(0)}\right) + \frac{2}{\beta}\frac{dh_t}{dx}{s_{xx}}^{(0)},\\
-2\frac{dg}{dx}{s_{xx}}^{(()}x, g(x)) + \beta {s_{xy}}^{(()}x, g(x)) &= -2\frac{dg}{dx}{S_{xx}}^{(()}x, g(x)) + \beta {S_{xy}}^{(()}x, g(x)),\\
-{\sigma_{yy}}^{(0)} + 2\frac{dg}{dx}{s_{xy}}^{(0)} - \left(\frac{dg}{dx}\right)^2{\sigma_{xx}}^{(0)} &= -{\Sigma_{yy}}^{(0)} + 2\frac{dg}{dx}{S_{xy}}^{(0)} - \left(\frac{dg}{dx}\right)^2{\Sigma_{xx}}^{(0)},\\
\text{and}\quad \frac{dP^{(0)}}{dx}h_t(x) + C_0 &= \beta\gamma_t\left(\beta P^{(0)} + {S_{xx}}^{(0)}\right) + \frac{2}{\beta}\frac{dh_t}{dx}{S_{xx}}^{(0)},
\end{aligned}
\tag{96}
$$

that solve for an ordinary differential equation for pressure,

$$
\frac{dp^{(0)}}{dx}\Delta h - \beta\Delta\gamma\beta p^{(0)} = \beta\Delta\gamma + \frac{2}{\beta}\left(\frac{dh_t}{dx} - K\frac{dh_b}{dx}\right); \tag{97}
$$

a relation between the pressures of the top and bottom materials,

$$
P^{(0)} = p^{(0)} + \frac{1-K}{\beta}; \tag{98}
$$

and equations for both shears in terms of the previously solved pressure and longitudinal stresses,

$$
\begin{aligned}
{s_{xy}}^{(0)} &= \frac{1}{\Delta h}\left(\beta\Delta\gamma\left(\beta p^{(0)}+1\right) + \frac{2}{\beta}\left(\frac{dh_t}{dx} - K\frac{dh_b}{dx}\right)\right)(y-h_t) + \beta\gamma_t\left(\beta p^{(0)}+1\right) + \frac{2}{\beta}\frac{dh_t}{dx},\\
{S_{xy}}^{(0)} &= \frac{1}{\Delta h}\left(\beta\Delta\gamma\left(\beta p^{(0)}+1\right) + \frac{2}{\beta}\left(\frac{dh_t}{dx} - K\frac{dh_b}{dx}\right)\right)(y-h_b) + \beta\gamma_b\left(\beta p^{(0)}+1\right) + \frac{2}{\beta}K\frac{dh_b}{dx}.
\end{aligned}
\tag{99}
$$

8 Conclusion and Future Work

Thus far models have been developed for both symmetric and weakly asymmetric rolling in a thin-sheet regime. It has been demonstrated with strain rate hardening, clad sheet rolling, Coulomb friction and relative-slip friction that alternative material and friction models can be used. Limitations of modelling assumptions, particularly larger friction regimes, have been found that provide evidence to which phenomena become significant under these assumptions.

Some preliminary numerical validation has been performed which shows some promising results such as the good agreement of trends in figure 14, but the use of the commerical *ABAQUS* package is limiting. There is an inability to completly turn off certain behaviours, such as elasticity, so the source of descrepancies can not be determined from additional phenomena in the numerical simulation, poor asymptotic assumptions or implementation error.

Issues also arise when performing calculations with extreme parameters choices such as increasing the elastic modulus which leads to stability issues. Convergence tests such as figure 8 also face issues as δ to approaches zero. Sparse relative dimensions like this require many small elements to ensure mesh convergence but this results in large numerical models and small time steps so computation times become unpractical.

Producing a bespoke numerical solver to solve the exact governing equations used in each model would ensure only the desired phenomena are included. Scaling these equations by the roll gap geometry would also allow solutions to be efficiently calculated in the limit of δ approaching zero. This would validate the correctness of the asymptotic models and provide some quantification of the error as each parameter is varied.

After the completion of the *Cambridge University Engineering Department* rolling machine, or from collaboration with another laboratory such as the University of Aachen, experimental comparison would provide the ultimate validation. This also has scope for a quantitative review of the models available in literature. Completing additional rows or columns of table 1 to compare the impact and significance of material and friction models could enhance this review.

8.0.1 Moments and Curvature

The assumption of vertical boundaries to the region undergoing plastic deformation is an obvious assumption to question, especially if bending moments are included. In fact, numerical simulations suggest that plasticity begins on a nearly triangular boundary into the roll gap. A brief investigation was carried out to parameterise the boundary to approximate this shape and accommodate bending. The approximation is illustrated in figure 15 where the new parameters, a and b, define the geometry.

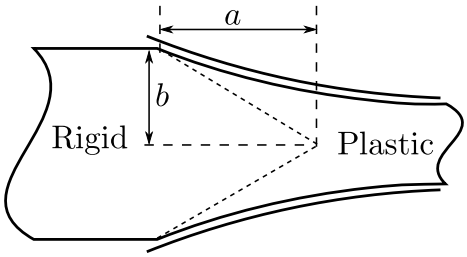

Figure 15: Illustration of a non-square plastic region within the roll gap parameterised by a and b.

These were to be solved, along with the longitudinal stress end condition, by considering the moment and both horizontal and vertical force on the end of the workpiece. Unfortunately the vertical force remains identically zero which leaves one degree of freedom in the parameterisation. Moments supported by this method, and those resulting from asymmetries, appear small when curvature is calculated using the method presented in Salimi and Sassani [2002]. Both the movement of the tri-junctions along the roll surface and elasticity could be significant in accounting for more general end forces and larger moments. The tri-junctions would break the symmetry in the leading order vertical force boundary condition and elasticity would be necessary to more accurately match the outer workpiece with the inner plastic region as the higher orders of correction already fail to satisfy rigid body motion at either end of the roll bite. A model that transitions between elastic and plastic deformation would be ideal as this could accommodate an arbitrary plastic region boundary.

8.0.2 Coupling Additional Physics

Similar to the strain-rate hardening and clad sheet rolling, many opportunities exist to incorporate more complex physics and phenomena into the models.

Roller deformation is a major concern for the regime these models describe: cold, thin-sheet rolling. There is a possibility to incorporate a simple elastic roller model into the asymptotic analysis.

Temperature would be another interesting addition to the model, especially in support of the *Cambridge University Engineering Department* rolling machine. However, this is likely a challenging proposition. Temperature is tightly coupled with heating from deformation energy and material properties dependent on temperature.

8.1 Other Processes

8.1.1 Ring Rolling

Ring rolling, for which there are few analytical models, provides an opportunity to combine other mathematical approaches with the asymptotic rolling presented here. The slow closure of the roll gap as the ring passes through many times produces near circularity in the ring. This lends itself to a weakly non-axisymmetric, multiple timescales approach where an outer elastic model of the ring is matched to the inner roll bite solution.

This would create two major challenges in modelling the roll bite. The first is the significant moments that act as boundary conditions to the roll gap; these are coupled entry to exit by the outer problem. For example hoop stresses would build in the ring. The second is the aspect ratio of rings are often much thicker than the regimes presented here: as much as ten times thicker than longer. This may be sufficiently thick to utilise a boundary-layer approach to model the effect of the rolls. Matched asymptotics may then be sufficient to find a model to approximate the entire operating regime.

Using an alternative approximate, empirical or even numerical solution to the inner problem may also lead to some useful results, such as stability conditions, when matched to the outer problem.

8.1.2 English Wheel

Another exciting modelling application is the English wheel. The English wheel uses a rolling setup of limited width to locally thin a sheet. The thinning requires the material to spread laterally which will force out of plane deformation and create curvature in the sheet. Figure 16 is a picture of the English wheel with a doubly curved workpiece. There is a second, bottom, roll hidden by the workpiece.

Figure 16: Picture of an English wheel with a doubly curved workpiece.

Like ring rolling, this model could match an outer problem to the inner asymptotic rolling problem. In this case, the outer solution would be a shell model, used to determine the residual stresses and out of plane deformation of the sheet. This would provide geometry and force boundary conditions for the inner problem that would determine the localised effect of tooling. This may be sufficient to generate a work path for process automation for which no solution currently exists in literature.

It is an application that exists closer to the small aspect ratio regime but requires the extension to three dimensions. Ensuring compatibility span-wise will require some consideration of elastic effects but, similar to the ring rolling model, other solution methods could be matched to an outer solution.

References

J.M. Alexander. A Slip Line Field for the Hot Rolling Process. *Proceedings of the Institution of Mechanical Engineers*, 169:1021, 1955. doi: 10.1243/PIME.

J.M. Alexander. On the Theory of Rolling. *Proceedings of the Royal Society A: Mathematical, Physical and Engineering Sciences*, 326(1567):535–563, February 1972. ISSN 1364-5021. doi: 10.1098/rspa.1972.0025. URL `http://rspa.royalsocietypublishing.org/cgi/doi/10.1098/rspa.1972.0025`.

D. R. Bland and Hugh Ford. The calculation of roll force and torque in cold strip rolling with tensions. *Proceedings of the Institution of Mechanical Engineers*, 159:144, June 1948a. doi: 10.1243/PIME. URL `http://pme.sagepub.com/content/159/1/144.short`.

D.R. Bland and H. Ford. An approximate treatment of the elastic compression of the strip in cold rolling. *Journal of Iron Steel Institute*, 171:245–249, 1948b.

S. A. E. Buxton and S. C. Browning. Turn-up and Turn-down in Hot Rolling: A Study on a Model Mill Using Plasticine. *Journal of Mechanical Engineering Science*, 14(4):245–254, 1972. doi: 10.1243/JMES.

A. P. Chekmarev and A.A. Nefedov. No Title. *Obrabotka Metallov Davleniem*, 4:2–15, 1956. URL `(British Library Translation R.T.S. 8939)`.

H.P. Cherukuri, Robert E. Johnson, and R.E. Smelser. A Rate-Dependent Model for Hot-Rolling. *International Journal of Mechanical Sciences*, 39(6):705–727, 1997.

Ian F. Collins. Slipline Field Solutions for Compression and Rolling with Slipping Friction. *International Journal of Mechanical Sciences*, 11:971–978, 1969.

Ian F. Collins and P. Dewhurst. A Slipline Field Analysis of Asymmetrical Hot Rolling. *International Journal of Mechanical Sciences*, 17:643–651, 1975.

S.A. Dassault Systemes. Abaqus 6.12 Example Problems Manual, 2012.

P. Dewhurst, I.F. Collins, and W. Johnson. A theoretical and experimental investigation into asymmetrical hot rolling. *International Journal of Mechanical Sciences*, 16(6):389–397, June 1974. ISSN 00207403.

S.A. Domanti and D. L. S. McElwain. Two-Dimensional Plane Strain Rolling: An Asymptotic Approach to the Estimation of Inhomogeneous Effects. *International Journal of Mechanical Sciences*, 37(2): 175–196, 1995.

S.A. Domanti and D.L.S. McElwain. Cold rolling of flat metal products: contribution of mathematical modelling. *Proceedings of the Institution of Mechanical Engineers, Part B: Journal of Engineering Manufacture*, 212(1):73–86, January 1998. ISSN 0954-4054. doi: 10.1243/0954405981515518. URL `http://pib.sagepub.com/lookup/doi/10.1243/0954405981515518`.

S.A. Domanti, D.L.S. McElwain, and R.H. Middleton. Model of cold rolling of thin metal sheets between nonparallel rolls. 18(July), 1994.

M. I. Ghobrial. A Photoelastic Investigation on the Contact Stresses Developed in Rolls During Asymmetrical Flat Rolling. *International Journal of Mechanical Sciences*, 31(10):751–764, 1989.

R.M. Govindarajan and N Aravas. Asymptotic Analysis of Extrusion of Porous Metals. *Journal of Mechanical Science*, 33(7):505–527, 1991.

P. Hartley, C.E.N Sturgess, C. Liu, and G.W. Rowe. Experimental and Theoretical Studies of Workpiece Deformation, Stress, and Strain During Flat Rolling. *International Materials Reviews*, 34(1):19–34, 1989.

Yeong-Maw Hwang and Gow-Yi Tzou. An Analytical Approach to Asymmetrical Cold- and Hot-Rolling of Clad Sheet Using the Slab Method. *Journal of Materials Processing Technology*, 62:249–259, 1996.

Robert E. Johnson. Conical extrusion of a work-hardening material: an asymptotic analysis. *Journal of Engineering Mathematics*, 21(4):295–329, 1987. ISSN 0022-0833. doi: 10.1007/BF00132681. URL http://link.springer.com/10.1007/BF00132681.

Robert E. Johnson. Shape Forming and Lateral Spread in Sheet Rolling. *International Journal of Mechanical Sciences*, 33(6):449–469, 1991.

Robert E. Johnson. The Effect of Friction and Inelastic Deformation on Chatter in Sheet Rolling. *Proceedings of the Royal Society A: Mathematical, Physical and Engineering Sciences*, 445(1925):479–499, June 1994a. ISSN 1364-5021. doi: 10.1098/rspa.1994.0073. URL http://rspa.royalsocietypublishing.org/cgi/doi/10.1098/rspa.1994.0073.

Robert E. Johnson. Cold Sheet Rolling with Unequal Friction at the Roll-Sheet Interfaces. In *Manufacturing Science and Engineering*, volume 68, pages 619–626, 1994b.

Robert E. Johnson and R.G. Keanini. An asymptotic model of work roll heat transfer in strip rolling. *International Journal of Mass Transfer*, 41:871–879, 1998.

Robert E. Johnson and R.E. Smelser. An asymptotic formulation of shear effects in two dimensional rolling. *Journal of Materials Processing Technology*, 34:311–318, 1992.

W. Johnson and G. I. Needham. Further Experiments in Asymmetrical Rolling. *International Journal of Mechanical Sciences*, 8:443–455, June 1966.

M.E. Karabin and R.E. Smelser. A quasi-three-dimensional analysis of the deformation processing of sheets with applications. *International Journal of Mechanical Sciences*, 32(5): 375–389, January 1990. ISSN 00207403. doi: 10.1016/0020-7403(90)90167-H. URL http://linkinghub.elsevier.com/retrieve/pii/002074039090167H.

T.von Karman. Zeit.Ang. *Zeitschrift fur angewandte Mathematik und Mechanik*, 5:142, 1925.

G.E. Kennedy and F. Slamar. Turn-up and Turn-down in Hot Rolling. *Iron and Steel Engineer*, 35:71, 1958.

M. M. Kiuchi and S. Hsiang. Analytical Model of Asymmetrical Rolling Process of Sheets. *Proceedings of the 14th NAMRC, Society of Manufacturing Engineers, Minneapolis*, page 384, 1986.

C. W. Knight, S. J. Hardy, A. W. Lees, and K. J. Brown. Influence of roll speed mismatch on strip curvature during the roughing stages of a hot rolling mill. *Journal of Materials Processing Technology*, 168(1):184–188, September 2005. ISSN 09240136.

T.A.M. Langlands and D.L.S. McElwain. A modifed Hertzian foil rolling model : approximations based on perturbation methods. 44:1715–1730, 2002.

Jerzy Mischke. Equations of Strip Equilibrium During Asymmetrical Flat Rolling. *Journal of Materials Processing Technology*, 61:382–394, 1996.

Pierre Montmitonnet. Hot and cold strip rolling processes. *Computer Methods in Applied Mechanics and Engineering*, 195(48-49):6604–6625, October 2006. ISSN 00457825. doi: 10.1016/j.cma.2005.10.014. URL http://linkinghub.elsevier.com/retrieve/pii/S0045782505004779.

Pierre Montmitonnet and P. Buessler. A Review on Theoretical Analyses of Rolling in Europe. 31(6): 525–538, 1991.

A. Nadai. "Plasticity". *Journal of Applied Mechanics1*, 6:A–55, 1931.

E Orowan. The calculation of roll pressure in hot and cold flat rolling. *Proceedings of the Institution of Mechanical Engineers*, 150:140–167, July 1943. ISSN 0020-3483. doi: 10.1243/PIME_PROC_1943_150_025_02. URL http://pme.sagepub.com/lookup/doi/10.1243/PIME_PROC_1943_150_025_02.

E Orowan and K.J. Pascoe. *First Report of the Rolling-Mill Research Sub-Committee*. Iron and Steel Institute, London, 1946.

D. Pan and D. H. Sansome. An Experimental Study of the Effect of Roll-Speed Mismatch on the Rolling Load During the Cold Rolling of Thin Strip. *Journal of Mechanical Working Technology*, 6:361–377, 1982.

Ann Bettina Richelsen. Elastic-Plastic Analysis of the Stress and Strain Distributions in Asymmetric Rolling. *International Journal of Mechanical Sciences*, 39(11):1199–1211, 1997.

G Sachs and L. J. Klinger. The Flow of Metals through Tools of Circular Contour. *Trans. ASME, Journal of Applied Mechanics*, 69:88–98, 1947.

M. Salimi and F. Sassani. Modified slab analysis of asymmetrical plate rolling. *International Journal of Mechanical Sciences*, 44:1999–2023, 2002.

R. Sauer and O. Pawelski. Theoretical study of the effect of asymmetries on the cold rolling process. *Steel Res.*, 58(7):319–326, 1987.

R. Shivpuri, P. C. Chou, and C. W. Lau. Finite Element Investigation of Curling in Non-Symmetric Rolling of Flat Stock. *International Journal of Mechanical Sciences*, 30(9):625–635, 1988.

E. Siebel. Berichte des Walzwerksausschusses. *Verein deutsher Eisenhuttenleute*, 37:1–4, 1924.

E. Siebel. Zur theories des walzvoganges bei ungleich angetriebenen walzen. *Archiv fur das Eisenhuettenwesen*, 15:125, 1941.

E. Siebel and A. Pomp. Mitteilungen aus dem Kaiser. *Mitteilungen aus dem Kaiser Wilhelm Institut fur Eisenforshung, Dussledorf*, 9:157, 1927.

Robert P Smet and Robert E. Johnson. An Asymptotic Analysis of Cold Sheet Rolling. *Journal of Applied Mechanics*, 56(March 1989):33–39, 1989.

R. D Venter and A Abd-Rabbo. Modelling of the Rolling Process I: Inhomogeneous Deformation Model. *International Journal of Mechanical Sciences*, 22(2):83–92, 1980.

R. D Venter and A Adb-Rabbo. Modelling of the Rolling Process II: Evaluation of the Stress Distribution in the Rolled Material. 22:93–98, 1980.

A Friction Boundaries

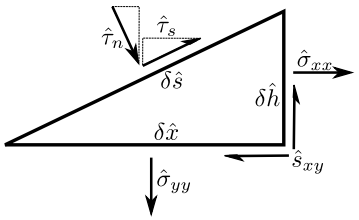

Figure 17: Figure showing the forces acting on an arbitrary boundary element

Take a horizontal and vertical force balance, of the forces acting on an elemental boundary volume, figure 17,

$$\delta\hat{h}\hat{\sigma}_{xx} - \delta\hat{x}\hat{s}_{xy} + \delta\hat{h}\hat{\tau}_n + \delta\hat{x}\hat{\tau}_s = 0$$
$$\delta\hat{x}\hat{\sigma}_{yy} - \delta\hat{h}\hat{s}_{xy} + \delta\hat{x}\hat{\tau}_n - \delta\hat{h}\hat{\tau}_s = 0.$$

Dividing through by $\delta\hat{x}$ and taking the limit $\hat{x} \to 0$ gives

$$\frac{d\hat{h}}{d\hat{x}}\hat{\sigma}_{xx} - \hat{s}_{xy} + \frac{d\hat{h}}{d\hat{x}}\hat{\tau}_n + \hat{\tau}_s = 0$$
$$\hat{\sigma}_{yy} - \frac{d\hat{h}}{d\hat{x}}\hat{s}_{xy} + \hat{\tau}_n - \frac{d\hat{h}}{d\hat{x}}\hat{\tau}_s = 0.$$

This result can equally be obtained by considering a rotation of the stress tensor.

Rearranging these equations gives the traction normal and shear stress,

$$\hat{\tau}_n = \frac{1}{1+\left(\frac{d\hat{h}}{d\hat{x}}\right)^2}\left(-\hat{\sigma}_{yy} + 2\frac{d\hat{h}}{d\hat{x}}\hat{s}_{xy} - \left(\frac{d\hat{h}}{d\hat{x}}\right)^2\hat{\sigma}_{xx}\right)$$
$$\hat{\tau}_s = \frac{1}{1+\left(\frac{d\hat{h}}{d\hat{x}}\right)^2}\left(\frac{d\hat{\hat{h}}}{d\hat{x}}\left(\hat{\sigma}_{yy}-\hat{\sigma}_{xx}\right) + \hat{s}_{xy}\left(1-\left(\frac{d\hat{h}}{d\hat{x}}\right)^2\right)\right),$$

or, using the plane strain result, more usefully reduced to

$$\hat{s}_{xy} = \hat{\tau}_s\left(1+\left(\frac{d\hat{h}}{d\hat{x}}\right)^2\right) - 2\hat{s}_{xx}\frac{d\hat{h}}{d\hat{x}} + \hat{s}_{xy}\left(\frac{d\hat{h}}{d\hat{x}}\right)^2.$$

Non-dimensionalising this result with the scalings used in section 5 gives

$$s_{xy}(x,h(x)) = \tau(x)\left(1+\delta^2\left(\frac{dh}{dx}\right)^2\right) - \frac{2}{\beta}\frac{dh}{dx}s_{xx}(x,h(x)) + \delta^2 s_{xy}(x,h(x))\left(\frac{dh}{dx}\right)^2.$$

This can be repeated for a bottom boundary element, or noticing that reflection will change the sign of the shear terms, τ_s and s_{xy},

$$s_{xy}(x,h_b(x)) = \tau_b(x)\left(1+\delta^2\left(\frac{dh_b}{dx}\right)^2\right) + \frac{2}{\beta}\frac{dh_b}{dx}s_{xx}(x,h_b(x)) + \delta^2 s_{xy}(x,h_b(x))\left(\frac{dh_b}{dx}\right)^2.$$

Applying a friction model provides another equation for $\hat{\tau}_s$ which gives a boundary condition in terms of the stress variables only.

A.1 Coulomb Friction

Coulomb friction defines the surface shear as proportional to the surface normal stress, or

$$\hat{\tau}_s = \frac{\Delta\mathbf{u}}{|\Delta\mathbf{u}|}\hat{\mu}\hat{\tau}_n.$$

Substituting the previous expansions, non-dimensionalising and expanding to each order gives the boundary conditions

$$\begin{aligned}
{s_{xy}}^{(0)}(x,h_t(x)) &= \frac{\Delta\mathbf{u}}{|\Delta\mathbf{u}|}\frac{\mu}{\bar{\beta}}\frac{\bar{\beta}}{\delta}p^{(0)}(x,h_t(x)) + \frac{\mu}{\bar{\beta}}\frac{\Delta\mathbf{u}}{|\Delta\mathbf{u}|}{s_{xx}}^{(0)}(x,h_t(x)) - \frac{2\delta}{\bar{\beta}}{s_{xx}}^{(0)}(x,h_t(x))\frac{dh_t(x)}{dx},\\
{s_{xy}}^{(1)}(x,h_t(x)) &= 0,\\
{s_{xy}}^{(2)}(x,h_t(x)) &= \gamma_t\beta p^{(2)}(x,h_t(x)) - \left(\frac{2}{\beta}\frac{dh_t}{dx}+1\right){s_{xx}}^{(2)}\\
&\quad + \left(\frac{dh_t}{dx}\right)^2\left(\gamma_t\left(\beta p^{(0)}(x,h_t(x)) - {s_{xx}}^{(0)}(x,h_t(x))\right) + {s_{xy}}^{(0)}(x,h_t(x))\left(1+2\gamma_t\beta\frac{dh_t}{dx}\right)\right),\\
{s_{xy}}^{(0)}(x,h_b(x)) &= \frac{\Delta\mathbf{u}}{|\Delta\mathbf{u}|}\frac{\mu}{\bar{\beta}}\frac{\bar{\beta}}{\delta}p^{(0)}(x,h_b(x)) + \frac{\mu}{\bar{\beta}}\frac{\Delta\mathbf{u}}{|\Delta\mathbf{u}|}{s_{xx}}^{(0)}(x,h_b(x)) + \frac{2\delta}{\bar{\beta}}{s_{xx}}^{(0)}(x,h_b(x))\frac{dh_b(x)}{dx},\\
\text{and}\quad {s_{xy}}^{(2)}(x,h_b(x)) &= \gamma_b\beta p^{(2)}(x,h_b(x)) - \left(\frac{2}{\beta}\frac{dh_b}{dx}+1\right){s_{xx}}^{(2)}\\
&\quad + \left(\frac{dh_b}{dx}\right)^2\left(\gamma_b\left(\beta p^{(0)}(x,h_b(x)) - {s_{xx}}^{(0)}(x,h_b(x))\right) + {s_{xy}}^{(0)}(x,h_b(x))\left(1+2\gamma_b\beta\frac{dh_b}{dx}\right)\right).
\end{aligned} \tag{100}$$

A.2 Relative-Slip Friction

Relative-slip defines the surface shear as proportional to the difference in velocities between the two surfaces, or

$$\hat{\tau}_s = \hat{\kappa}\left(\hat{u}_s - \hat{U}\right)$$

where, using the velocity boundary condition,

$$\begin{aligned}\hat{u}_s &= \sqrt{\hat{u}^2 + \hat{v}^2} \\ &= \sqrt{\hat{u}^2\left(1 + \left(\frac{d\hat{h}}{d\hat{x}}\right)^2\right)}.\end{aligned}$$

Combined with the earlier result, the shear condition is

$$\hat{s}_{xy} = \hat{\kappa}\left(\hat{u} - \hat{U}\right) - 2\frac{d\hat{h}}{d\hat{x}}\hat{s}_{xx} + \left(\frac{\hat{\kappa}\hat{u}}{2} + 2\hat{s}_{xy} + \hat{\kappa}\left(\hat{u} - \hat{U}\right)\right)\left(\frac{d\hat{h}}{d\hat{x}}\right)^2 + O\left(\left(\frac{d\hat{h}}{d\hat{x}}\right)^4\right).$$

Non-dimensionalising and expanding to each order gives

$$\begin{aligned}&{s_{xy}}^{(0)}(x, h_t(x)) = \frac{u^{(0)}(x, h_t(x)) - U_t}{\Delta U} - \frac{2}{\beta}\frac{dh_t}{dx} = \frac{2 - U_t\Delta h}{\Delta h \Delta U} - \frac{2}{\beta}\frac{dh_t}{dx}, \\ &{s_{xy}}^{(1)}(x, h_t(x)) = 0, \\ &{s_{xy}}^{(0)}(x, h_b(x)) = -\kappa\frac{u^{(0)}(x, h_b(x)) - U_b}{\Delta U} - \frac{2}{\beta}\frac{dh_b}{dx} = -\kappa\frac{2 - U_b\Delta h}{\Delta h \Delta U} - \frac{2}{\beta}\frac{dh_t}{dx}, \\ \text{and}\quad &{s_{xy}}^{(1)}(x, h_b(x)) = 0.\end{aligned}$$

B Asymmetric, $\bar{\beta} = O(\delta)$, Perfect Plastic $O(\delta^2)$ Solution with Coulomb Friction

Continuing the expansion of the asymmetric, small firction, perfect plastic solution with coulomb friction in section 5.2.1, we begin by outlining the second order governing equations and boundary conditions. The equations after removing the first order solutions that were found to be zero are

$$-\beta\frac{\partial p^{(2)}}{\partial x} + \frac{\partial {s_{xx}}^{(2)}}{\partial x} + \beta\frac{\partial {s_{xy}}^{(2)}}{\partial y} = 0, \tag{101}$$

$$-\beta\frac{\partial p^{(2)}}{\partial y} - \frac{\partial {s_{xx}}^{(2)}}{\partial y} + \beta\frac{\partial {s_{xy}}^{(0)}}{\partial x} = 0, \tag{102}$$

$$\frac{\partial u^{(2)}}{\partial x} = \lambda^{(0)}{s_{xx}}^{(2)} + \lambda^{(2)}{s_{xx}}^{(0)}, \tag{103}$$

$$\frac{\partial v^{(2)}}{\partial x} = -\lambda^{(0)}{s_{xx}}^{(2)} - \lambda^{(2)}{s_{xx}}^{(0)}, \tag{104}$$

$$\frac{\partial u^{(2)}}{\partial y} + \frac{\partial v^{(0)}}{\partial x} = 2\beta\lambda^{(0)}{s_{xy}}^{(0)}, \tag{105}$$

$$\frac{\partial u^{(2)}}{\partial x} + \frac{\partial v^{(2)}}{\partial y} = 0, \tag{106}$$

$$\text{and}\quad 4{s_{xx}}^{(0)}{s_{xx}}^{(2)} + 2\beta^2{s_{xy}}^{(0)2} = 0, \tag{107}$$

$$\tag{108}$$

and the boundary conditions are

$$
\begin{aligned}
{s_{xy}}^{(2)}(x,h_t(x)) &= \gamma_t\beta p^{(2)}(x,h_t(x)) - \left(\frac{2}{\beta}\frac{dh_t}{dx}+1\right){s_{xx}}^{(2)} \\
&+ \left(\frac{dh_t}{dx}\right)^2\left(\gamma_t\left(\beta p^{(0)}(x,h_t(x)) - {s_{xx}}^{(0)}(x,h_t(x))\right) + {s_{xy}}^{(0)}(x,h_t(x))\left(1+2\gamma_t\beta\frac{dh_t}{dx}\right)\right), \\
{s_{xy}}^{(2)}(x,h_b(x)) &= \gamma_b\beta p^{(2)}(x,h_b(x)) - \left(\frac{2}{\beta}\frac{dh_b}{dx}+1\right){s_{xx}}^{(2)} \\
&+ \left(\frac{dh_b}{dx}\right)^2\left(\gamma_b\left(\beta p^{(0)}(x,h_b(x)) - {s_{xx}}^{(0)}(x,h_b(x))\right) + {s_{xy}}^{(0)}(x,h_b(x))\left(1+2\gamma_b\beta\frac{dh_b}{dx}\right)\right). \qquad (109)
\end{aligned}
$$

(110)

$$
\begin{aligned}
\int_{h_b(0)}^{h_t(0)} -\beta p^{(2)}(0,y) + {s_{xx}}^{(2)}(0,y)dy &= 0, \\
\int_{h_b(1)}^{h_t(1)} -\beta p^{(2)}(1,y) + {s_{xx}}^{(2)}(1,y)dy &= 0, \qquad (111) \\
\int_{h_b(x)}^{h_t(x)} u^{(2)}(x,y)dy &= 0, \qquad (112) \\
v^{(2)}(x,h_t(x)) &= \frac{dh_t(x)}{dx}u^{(2)}(x,h_t(x)) \\
\text{and} \quad v^{(2)}(x,h_b(x)) &= \frac{dh_b(x)}{dx}u^{(2)}(x,h_b(x)). \qquad (113)
\end{aligned}
$$

Begin by determining the velocities. The second order correction to the horizontal velocity can be determined by integrating equation (105) with respect to y. This produces

$$u^{(2)} = 2\beta\lambda^{(0)}\int {s_{xy}}^{(0)}dy - \int\frac{\partial v^{(0)}}{\partial x}dy + c_0(x)$$

where the constant function $c_0(x)$, can be determined with equation (112), ultimately leading to

$$
\begin{aligned}
u^{(2)}(x,y) = \frac{2\beta}{\Delta h^2}\frac{d\Delta h}{dx}&\left(\Delta\gamma\left(\frac{\Delta h^2}{6}-\frac{y^2}{2}\right)+(\gamma_t h_b-\gamma_b h_t)\left(\frac{\Delta h}{2}-y\right)\right) \\
&+\left(\frac{-4}{\Delta h^3}\frac{d\Delta h}{dx}\left(h_t\frac{dh_b}{dx}-h_b\frac{dh_t}{dx}\right)+\left(h_t\frac{d^2h_b}{dx^2}-h_b\frac{d^2h_t}{dx^2}\right)\right)\left(\frac{\Delta h}{2}-y\right) \\
&-\left(\frac{4}{\Delta h^2}\left(\frac{d\Delta h}{dx}\right)^2+\frac{d^2\Delta h}{dx^2}\right)\left(\frac{\Delta h^2}{6}-\frac{y^2}{2}\right) \qquad (114)
\end{aligned}
$$

It proves useful to calculate

$$\begin{aligned}\frac{\partial v^{(2)}}{\partial x} = \frac{2\beta}{\Delta h^3}&\left(\frac{d^2\Delta h}{dx^2}\left(\beta p^{(0)}+1\right)+\frac{d\Delta h}{dx}\beta\frac{dp^{(0)}}{dx}-\left(\frac{d\Delta h}{dx}\right)^2\frac{3\left(p^{(0)}+1\right)}{\Delta h}\right)\\ &\left(\Delta\gamma\left(\frac{\Delta h^2}{6}-\frac{y}{3}\right)+\left(\gamma_t h_b-\gamma_b h_t\right)\left(\frac{\Delta h}{2}-y\right)\right)\\ &+\frac{2\beta}{\Delta h^3}\frac{d\Delta h}{dx}\left(\beta p^{(0)}+1\right)\left(\Delta\gamma\frac{\Delta h}{3}\frac{d\Delta h}{dx}+\left(\gamma_t\frac{dh_b}{dx}-\delta_b\frac{dh_t}{dx}\right)\left(\frac{\Delta h}{2}-y\right)+\left(\gamma_t h_b-\gamma_b h_t\right)\frac{1}{2}\frac{d\Delta h}{dx}\right)\\ &+\left(\frac{4}{\Delta h^3}\left(\frac{3}{\Delta h}\left(\frac{d\Delta h}{dx}\right)^2-\frac{d^2\Delta h}{dx^2}\right)\left(h_t\frac{dh_b}{dx}-h_b\frac{dh_t}{dx}\right)-\frac{4}{\Delta h^3}\frac{d\Delta h}{dx}\left(h_t\frac{d^2h_b}{dx^2}-h_b\frac{d^2h_t}{dx^2}\right)\right.\\ &\left.+\left(\frac{dh_t}{dx}\frac{d^2h_b}{dx^2}+h_t\frac{d^3h_b}{dx^3}-\frac{dh_t}{dx}\frac{d^2h_t}{dx^2}-h_b\frac{d^3h_t}{dx^3}\right)\right)\left(\frac{\Delta h}{2}-y\right)\\ &+\left(\left(h_t\frac{d^2h_b}{dx^2}-h_b\frac{d^2h_t}{dx^2}\right)-\frac{4}{\Delta h^3}\frac{d\Delta h}{dx}\left(h_t\frac{dh_b}{dx}-h_b\frac{dh_t}{dx}\right)\right)\frac{1}{2}\frac{d\Delta h}{dx}\\ &-\left(\frac{4}{\Delta h^3}\left(2\frac{d\Delta h}{dx}\frac{d^2\Delta h}{dx^2}-\frac{3}{\Delta h}\left(\frac{d\Delta h}{dx}\right)^2\right)+\frac{d^2\Delta h}{dx^2}\right)\left(\frac{\Delta h^2}{6}-\frac{y^2}{2}\right)\\ &-\left(\frac{4}{\Delta h^3}\left(\frac{d\Delta h}{dx}\right)^2+\frac{d^2\Delta h}{dx^2}\right)\frac{\Delta h}{3}\frac{d\Delta h}{dx},\end{aligned}\tag{115}$$

where $\frac{dp^{(0)}}{dx} = \frac{s_{xy}{}^{(0)}}{\Delta h}$ from equation (74) at leading order, as differentiating $u^{(2)}$ with respect to x then integrating with respect to y gives the vertical velocity second order correction by equation (106),

$$v^{(2)} = \int \frac{\partial u^{(2)}}{\partial x} dy.$$

From equation (115) it is easy to see integration produces

$$\begin{aligned}v^{(2)} = &\int \frac{\partial u^{(2)}}{\partial x} dy\\ =&\frac{2\beta}{\Delta h^3}\left(\frac{d^2\Delta h}{dx^2}\left(\beta p^{(0)}+1\right)+\frac{d\Delta h}{dx}\beta\frac{dp^{(0)}}{dx}-\left(\frac{d\Delta h}{dx}\right)^2\frac{3\left(p^{(0)}+1\right)}{\Delta h}\right)\\ &\left(\frac{y\Delta\gamma}{6}\left(\Delta h^2-y^2\right)+\frac{y}{2}\left(\gamma_t h_b-\gamma_b h_t\right)\left(\Delta h-y\right)\right)\\ &+\frac{2\beta}{\Delta h^3}\frac{d\Delta h}{dx}\left(\beta p^{(0)}+1\right)\left(\Delta\gamma\frac{y\Delta h}{3}\frac{d\Delta h}{dx}+\frac{y}{2}\left(\gamma_t\frac{dh_b}{dx}-\delta_b\frac{dh_t}{dx}\right)\left(\Delta h-y\right)+\left(\gamma_t h_b-\gamma_b h_t\right)\frac{y}{2}\frac{d\Delta h}{dx}\right)\\ &+\left(\frac{4}{\Delta h^3}\left(\frac{3}{\Delta h}\left(\frac{d\Delta h}{dx}\right)^2-\frac{d^2\Delta h}{dx^2}\right)\left(h_t\frac{dh_b}{dx}-h_b\frac{dh_t}{dx}\right)-\frac{4}{\Delta h^3}\frac{d\Delta h}{dx}\left(h_t\frac{d^2h_b}{dx^2}-h_b\frac{d^2h_t}{dx^2}\right)\right.\\ &\left.+\left(\frac{dh_t}{dx}\frac{d^2h_b}{dx^2}+h_t\frac{d^3h_b}{dx^3}-\frac{dh_t}{dx}\frac{d^2h_t}{dx^2}-h_b\frac{d^3h_t}{dx^3}\right)\right)\frac{y}{2}\left(\Delta h-y\right)\\ &+\left(\left(h_t\frac{d^2h_b}{dx^2}-h_b\frac{d^2h_t}{dx^2}\right)-\frac{4}{\Delta h^3}\frac{d\Delta h}{dx}\left(h_t\frac{dh_b}{dx}-h_b\frac{dh_t}{dx}\right)\right)\frac{y}{2}\frac{d\Delta h}{dx}\\ &-\left(\frac{4}{\Delta h^3}\left(2\frac{d\Delta h}{dx}\frac{d^2\Delta h}{dx^2}-\frac{3}{\Delta h}\left(\frac{d\Delta h}{dx}\right)^2\right)+\frac{d^2\Delta h}{dx^2}\right)\frac{y}{6}\left(\Delta h^2-y^2\right)\\ &-\left(\frac{4}{\Delta h^3}\left(\frac{d\Delta h}{dx}\right)^2+\frac{d^2\Delta h}{dx^2}\right)\frac{y\Delta h}{3}\frac{d\Delta h}{dx}+c_1(x)\end{aligned}\tag{116}$$

The constant of integration must then be determined using the vertical boundary condition - although this is algebraic in terms of $u^{(2)}$ so can be computed numerically,

$$c_1(x) = \frac{dh_t}{dx}u^{(2)}(x,h_t(x)) - v^{(2)-}(x,h_t(x)) \tag{117}$$

where $v^{(2)-}(x,y) = v^{(2)}(x,y) - c_1(x)$ or the known terms of equation (116).

From here the second order correction to the flow rate parameter is simply calculated as

$$\lambda^{(2)} = \frac{1}{{s_{xx}}^{(0)}} \left(\frac{\partial u^{(2)}}{\partial x} + \lambda^{(0)} \frac{\beta^2 {s_{xy}}^{(0)2}}{{s_{xx}}^{(0)}} \right).$$

The second order correction to the longitudinal deviatoric stresses are also easily computed from equation (107) and are given as

$${s_{xx}}^{(2)} = -{s_{yy}}^{(2)} = \frac{-\beta^2 {s_{xy}}^{(0)2}}{2{s_{xx}}^{(0)}}$$

Substituting the results thus far into equation (102) reveals the form of $p^{(2)}$ as

$$\begin{aligned} p^{(2)} &= \int \frac{\partial {s_{xy}}^{(0)}}{\partial x} dy - \frac{{s_{xx}}^{(2)}}{2} \\ &= \frac{-\beta y}{\Delta h^2} \left(2\frac{d\Delta h}{dx} + \left(\beta p^{(0)} + {s_{xx}}^{(0)} \right) (\beta \Delta\gamma - 1) \right) \left(\Delta\gamma \frac{y}{2} + (\gamma_t h_b - \gamma_b h_t) \right) \\ &\quad - \frac{\beta y}{\Delta h} \left(\beta p^{(0)} + {s_{xx}}^{(0)} \right) \left(\gamma_t \frac{dh_b}{dx} - \gamma_b \frac{dh_t}{dx} \right) - \frac{{s_{xx}}^{(2)}}{\beta} + c_2(x) \end{aligned} \tag{118}$$

and using it in equation (101) shows the form of ${s_{xy}}^{(2)}$ to be

$$\begin{aligned} {s_{xy}}^{(2)} &= -2\frac{\beta}{\Delta h^3} \left(p^{(0)} + \frac{1}{\beta} \right) \left(\frac{d\Delta h}{dx} \right)^2 \left(\Delta\gamma \frac{y^3}{6} + (\gamma_t h_b - \gamma b h_t) \frac{y^2}{2} \right) \\ &\quad - \frac{\beta p^{(0)} + 1}{\Delta h} 2\frac{\beta}{\Delta h^3} \frac{d\Delta h}{dx} \left(\frac{\Delta\gamma}{2} \left(\Delta\gamma \frac{y^4}{4} + (\gamma_t h_b - \gamma_b h_t) \frac{y^3}{3} \right) + (\gamma_t h_b - \gamma_b h_t) \left(\Delta\gamma \frac{y^3}{3} + (\gamma_t h_b - \gamma_b h_t) \frac{y^2}{2} \right) \right) \\ &\quad + \frac{\beta}{\Delta h^2} (\gamma_t h_b - \gamma_b h_t) \left(\left(\frac{\beta p^{(0)} + 1}{\Delta h^2} \frac{d\Delta h}{dx} - \frac{\beta}{\Delta h} \frac{dp^{(0)}}{dx} \right) \left(\Delta\gamma \frac{y^3}{3} + (\gamma_t h_b - \gamma_b h_t) \frac{y^2}{2} \right) \right. \\ &\qquad \left. - \frac{\beta p^{(0)} + 1}{\Delta h} \left(\gamma_t \frac{dh_b}{dx} - \gamma_b \frac{dh_t}{dx} \right) \frac{y^2}{2} \right) \\ &\quad + \frac{\beta}{\Delta h^2} \left(\left(p^{(0)} \frac{1}{\beta} \right) \frac{d\Delta h}{dx} \frac{y^2}{2} + \frac{\beta p^{(0)} + 1}{\Delta h} \left(\Delta\gamma \frac{y^3}{3} + (\gamma_t h_b - \gamma_b h_t) \frac{y^2}{2} \right) \right) \left(\gamma_t \frac{dh_b}{dx} - \gamma_b \frac{dh_t}{dx} \right) \\ &\quad - \frac{1}{\Delta h} \left(\beta \frac{dp^{(0)}}{dx} - \frac{\beta p^{(0)} + 1}{\Delta h} \right) \left(\gamma_t \frac{dh_b}{dx} - \gamma_b \frac{dh_t}{dx} \right) \frac{y^2}{2} - \frac{\beta p^{(0)} + 1}{\Delta h} \left(\gamma_t \frac{d^2 h_b}{dx^2} - \gamma_b \frac{d^2 h_t}{dx^2} \right) \frac{y}{2} \\ &\quad + \frac{2\beta}{{s_{xx}}^{(0)}} \left(\frac{\beta p^{(0)} + 1}{\Delta h^2} \left(\beta \frac{dp^{(0)}}{dx} - \left(\beta p^{(0)} + 1 \right) \frac{d\Delta h}{dx} \right) \left(\Delta\gamma \frac{y^3}{3} + y^2 (\gamma_t h_b - \gamma_b h_t) + (\gamma_t h_b - \gamma_b h_t)^2 y \right) \right. \\ &\qquad \left. + \left(\frac{\beta p^{(0)} + 1}{\Delta h} \right)^2 \left(\Delta\gamma \frac{y^2}{2} + (\gamma_t h_b - \gamma_b h_t) y \right) \left(\gamma_t \frac{dh_b}{dx} - \gamma_b \frac{dh_t}{dx} \right) \right) \\ &\quad + \frac{dc_2(x)}{dx} y + c_3(x). \end{aligned} \tag{119}$$

It now remains to solve for $c_2(x)$ and $c_3(x)$ by applying the force boundary conditions. Applying each friction conidition to equation (119) and eliminating $c_3(x)$ leaves a differential equation for $c_2(x)$,

$$\begin{aligned} \frac{dc_2}{dx} \Delta h - \beta\Delta\gamma c_2(x) &= -\left({s_{xy}}^{(2)-}(x, h_t(x)) - {s_{xy}}^{(2)-}(x, h_b(x)) \right) \\ &\quad + \beta\Delta\gamma \left(\frac{\beta}{\Delta h^2} \left(\left(p^{(0)} + \frac{1}{\beta} \right) \frac{d\Delta h}{dx} - {s_{xy}}^{(0)} \right) \left(\Delta\gamma \frac{y^2}{2} + (\gamma_t h_b - \gamma_b h_t) y \right) \right. \\ &\qquad \left. - \frac{\beta p^{(0)} + 1}{\Delta h} \left(\gamma_t \frac{dh_b}{dx} - \gamma_b \frac{dh_t}{dx} \right) y + \frac{\beta {s_{xy}}^{(0)2}}{2{s_{xx}}^{(0)}} \right) \\ &\quad - \frac{2}{\beta} \frac{d\Delta h}{dx} {s_{xx}}^{(2)} + \left(\left(\frac{dh_t}{dx} \right)^2 \gamma_t - \left(\frac{dh_b}{dx} \right)^2 \gamma_b \right) \left(\beta p^{(0)} - {s_{xx}}^{(0)} \right) + 2\beta {s_{xy}}^{(0)} \left(\gamma_t \frac{dh_t}{dx} - \gamma_b \frac{dh_b}{dx} \right) \end{aligned} \tag{120}$$

where ${s_{xy}}^{(2)-} = {s_{xy}}^{(2)} - c_3(x)$.

Like the leading order, this can be solved piecewise with horizontal longitudinal stress continuity maintained by adjusting the neutral points. The initial conditions for the outer two regions are determined by the end tensions as

$$\begin{aligned} c_2(x) =& \frac{1}{\Delta h}\frac{\beta p^{(0)}+1}{\Delta h}\left(\left(\beta p^{(0)}+1\right)\left(\gamma_t h_b-\gamma_b h_t\right)^2\right. \\ & -\frac{h_t^2-h_b^2}{2}\left(\left(\gamma_t h_b-\gamma_b h_t\right)\left(\frac{\beta}{\Delta h}\frac{d\Delta h}{dx}-\left(\gamma_t h_b-\gamma_b h_t\right)-2\Delta\gamma\frac{\beta p^{(0)}+1}{\Delta h}\right)-\beta\left(\gamma_t\frac{dh_b}{dx}-\gamma_b\frac{dh_t}{dx}\right)\right) \\ & \left.-\frac{h_t^3-h_b^3}{3}\frac{\Delta\gamma}{2}\left(\frac{\beta}{\Delta h}\frac{d\Delta h}{dx}-\left(\gamma_t h_b-\gamma_b h_t\right)-2\Delta\gamma\frac{\beta p^{(0)}+1}{\Delta h}\right)-\frac{\Delta\gamma^2}{2}\frac{h_t^4-h_b^4}{4}\right)+F(x). \end{aligned} \tag{121}$$

Finally, substitute this back into equation (119) with one of the two friciton conditions for $c_3(x)$.